

1 **Composite Analysis of Large-Scale Environments Conducive to**
2 **West Pacific Polar/Subtropical Jet Superposition**

3 ZACHARY J. HANDLOS AND JONATHAN E. MARTIN *

University of Wisconsin - Madison, Madison, Wisconsin

* *Corresponding author address:* Jonathan E. Martin, University of Wisconsin - Madison, 1225 West Dayton St., Madison, WI 53706.

E-mail: jemart1@wisc.edu

ABSTRACT

4
5 Though considerable research attention has been devoted to examination of the Northern
6 Hemispheric polar and subtropical jet streams, relatively little has been directed toward
7 understanding the circumstances that conspire to produce the relatively rare vertical su-
8 perposition of these usually separate features. This study investigates the structure and
9 evolution of large-scale environments associated with jet superposition events in the North-
10 west Pacific.

11 An objective identification scheme, using NCEP/NCAR Reanalysis 1 data, is employed
12 to identify all jet superpositions in the West Pacific (30-40°N, 135-175°E) for boreal win-
13 ters (DJF) between 1979/80 - 2009/10. The analysis reveals that environments conducive
14 to West Pacific jet superposition share several large-scale features usually associated with
15 East Asian Winter Monsoon (EAWM) northerly cold surges, including the presence of an en-
16 hanced Hadley Cell like circulation within the jet entrance region. It is further demonstrated
17 that several EAWM indices are statistically significantly correlated with jet superposition
18 frequency in the West Pacific.

19 The life cycle of EAWM cold surges promotes interaction between tropical convection
20 and internal jet dynamics. Low potential vorticity (PV), high- θ_e air, appearing to be asso-
21 ciated with anomalous convection in the West Pacific lower latitudes, is advected poleward
22 towards the equatorward side of the jet in upper tropospheric isentropic layers resulting in
23 anomalous anticyclonic wind shear that accelerates the jet. This, along with geostrophic
24 cold air advection in the left jet entrance region that drives the polar tropopause downward
25 through the jet core, promotes the development of the deep, vertical PV wall characteristic of
26 superposed jets. A conceptual model synthesizing the results of this analysis is introduced.

1. Introduction

The Northern Hemisphere polar (PJ) and subtropical jet streams (STJ) are important elements in the large-scale circulation of the atmosphere and play a substantive role in the evolution of extratropical weather phenomena. In accord with thermal wind balance, the tropopause level PJ generally resides in the upper troposphere within regions of strong lower and middle tropospheric baroclinicity (Reiter 1963). The STJ is confined to the upper troposphere and is associated with less substantial baroclinicity. Furthermore, the STJ is located on the poleward side of the Hadley cell circulation (Krishnamurti 1961), and angular momentum transport from equatorial latitudes poleward towards the subtropics is a strong driver of the STJ. Several decades of inquiry have been directed toward understanding the dynamics driving the maintenance of these jet streams as well as their effects on the development and propagation of weather systems (e.g., Namias and Clapp 1949; Loewe and Radok 1950a,b; Yeh 1950; Koetswaram 1953; Mohri 1953; Koetswaram and Parthasarathy 1954; Newton 1954; Sutcliffe and Bannon 1954; Defant and Taba 1957; Krishnamurti 1961; Riehl 1962; Reiter 1963; Palmén and Newton 1969; Keyser and Shapiro 1986; Shapiro and Keyser 1990).

The fact that both the PJ and STJ are associated with strong gradients in tropopause height follows from consideration of the quasi-geostrophic potential vorticity (QGPV) equation, written as

$$q = \frac{1}{f_0} \nabla^2 \phi + f + \frac{\partial}{\partial p} \left(\frac{f_0}{\sigma} \frac{\partial \phi}{\partial p} \right) = \Lambda(\phi) + f \quad (1)$$

where ϕ is geopotential, f is the coriolis parameter, f_0 is a constant, σ is the static stability parameter and Λ is the second order linear differential operator $\Lambda = \frac{1}{f_0} \nabla^2 + \frac{\partial}{\partial p} \left(\frac{f_0}{\sigma} \right) \frac{\partial}{\partial p} + \frac{f_0}{\sigma} \frac{\partial^2}{\partial p^2}$ (Cunningham and Keyser 2004). The across-flow gradient of QGPV ($\frac{\partial q}{\partial n}$) is largest where the geostrophic wind (V_g) is largest since, from (1) and assuming f is constant,

$$\frac{\partial q}{\partial n} = \Lambda \left(\frac{\partial \phi}{\partial n} \right) = \Lambda(-fV_g). \quad (2)$$

50 Defant and Taba (1957), hereafter DT57, were among the first to recognize this physical
 51 relationship. They identified three tropopause “steps” in the Northern Hemisphere: “tropical,”
 52 “subtropical” and “polar” (Fig. 1). Both the PJ and STJ reside where the magnitude
 53 of the meridional gradient of tropopause height is large (Fig. 1b, recreated from DT57).
 54 The analysis of DT57 made it clear that there is often a separation in both altitude (Fig.
 55 1a) and latitude (Fig. 1b) between the two jet species.

56 While relatively rare, there are instances in which both the PJ and STJ become vertically
 57 superposed to form a single jet stream entity characterized by a deep tropopause wall that is
 58 bounded by two (rather than three) tropopause steps. An example of this “superposition”
 59 of the PJ and STJ can be seen in the north Atlantic Ocean in Fig. 1b as well as in the
 60 West Pacific region near Japan (DT57). It is clear that the subtropical tropopause step is
 61 essentially non-existent within these two regions, and thus a single jet separates the tropical
 62 tropopause from the polar tropopause. An unusually large horizontal gradient in tropopause
 63 height, along with the presence of a deep, nearly vertical tropopause wall, are the primary
 64 structural features associated with a superposed jet.

65 Very few prior studies have considered jet superposition events. Reiter (1961) and Reiter
 66 (1963) mention the possibility of PJ/STJ merger via vertical superposition of one jet stream
 67 on the other, with subsequent investigation of an example in Reiter and Whitney (1969).
 68 In that study, the authors investigate this phenomenon over the continental United States,
 69 stating that such merged jets do not seem to “behave” in the same manner as isolated PJ
 70 or STJ entities. A study by Mohri (1953) investigated PJ/STJ superposition in the West
 71 Pacific, representing the first such study (to our knowledge) that considered the occurrence
 72 of such an event in this region.

73 Recent work by Christenson (2013) and Winters and Martin (2014) has renewed investi-
 74 gation of vertical jet superposition events using an objective jet stream identification scheme

75 (see Section 2 for more details). Such events are defined as the *vertical* alignment of the PJ
76 and STJ within a grid point column. Christenson (2013) constructs a climatology of such
77 events, finding that while superpositions are extremely rare in the Northern Hemisphere,
78 the maximum frequency of occurrence of superpositions occurs during boreal winter (i.e.,
79 December, January and February).

80 Winters and Martin (2014) show that a superposition event was an integral component
81 of the 2010 Nashville, TN flood in the eastern United States. Other extreme weather events
82 have been found to be associated with vertical jet superposition (Christenson 2013), and
83 cursory re-examination of the synoptic environments identified in prior studies of signifi-
84 cant weather events suggests some of them may have been associated with jet superposition
85 (Hoskins and Berrisford 1988; Shapiro and Keyser 1990; Hakim et al. 1996; Bosart et al.
86 1996). Thus, understanding the physical processes involved in the development of jet su-
87 perpositions as well as their role in significant weather-producing environments has both
88 operational and phenomenological appeal.

89 To the best of our knowledge, *no prior studies outside of Mohri (1953) have extensively*
90 *investigated superposition events in the West Pacific.* Since vertical jet superposition events
91 are more common in the West Pacific during boreal winter than in any other region in the
92 Northern Hemisphere (Christenson 2013), a goal of any study dedicated to examining this
93 phenomenon is to determine why this region has more frequent superpositions. Therefore, the
94 goal of the present study is twofold. First, we wish to determine what large-scale features are
95 associated with West Pacific vertical jet superposition events during boreal winter. Second,
96 we seek to identify the physical mechanisms that most commonly lead to jet superposition
97 in this region.

98 The paper is organized as follows: In Section 2, the dataset and methodology employed
99 in constructing composite maps of West Pacific jet superpositions are described. Section
100 3 focuses on discussion of features that are associated with West Pacific vertical jet super-
101 positions. In Section 4, the evolution of those synoptic features and how their interactions

102 lead to jet superposition is discussed. A summary and discussion of the results are offered
103 in Section 5.

104 **2. Data and Methods**

105 *a. Data*

106 The NCEP/NCAR Reanalysis 1 data (Kalnay et al. 1996) are employed for all variables
107 and calculations utilized in this study. The data have a 2.5° horizontal grid spacing and
108 6-hourly temporal resolution. Data on both isobaric (unevenly spaced between 100-1000
109 hPa) and isentropic surfaces (interpolated every 5 K and examined in the 315-330 K and
110 340-355 K layers¹) are used. We focus on the months of December, January and February
111 (DJF) for all winters 1979/80 - 2009/10 (31 winters; leap days excluded).

112 *b. Jet Superposition Identification Scheme*

113 We adopt the jet identification scheme used in Christenson (2013) and Winters and
114 Martin (2014). The scheme is described with the aid of Fig. 2 which illustrates aspects of
115 two different cases over the Pacific. Separate PJ and STJ features are clearly illustrated
116 in the plan view in Fig. 2a. Figure 2b shows a vertical cross section through both jet
117 cores. The polar jet core, located at approximately 300 hPa, is largely contained within the
118 315-330K isentropic layer while the subtropical jet core, located at approximately 200 hPa,
119 occupies the 340-355K layer (Fig. 2b). Both the subtropical and polar jet cores lie at the
120 low potential vorticity (PV) edge of the strong horizontal PV gradient that separates the
121 upper troposphere from the lower stratosphere.

122 The scheme evaluates characteristics of the PV and wind speed distributions in each

¹The 315-330K and 340-355K layers were computed by averaging all levels between 315-330K and 340-355K, respectively.

123 grid column. Within the 315-330K (340-355K) layer, whenever $|\nabla PV|$ within the 1-3 PVU
124 channel exceeds or is equal to a threshold value² and the integrated wind speed in the 400-
125 100 hPa layer $\geq 30 \text{ m s}^{-1}$, we identify a polar (subtropical) jet in that grid column. The
126 occurrence of both polar and subtropical jet characteristics in a single grid column identifies
127 a jet superposition event at that time in that grid column. An example vertical cross section
128 through an identified jet superposition³ (Fig. 2c) is shown in Fig. 2d. Notice the steepness
129 of the dynamic tropopause - a nearly vertical PV wall extends from ~ 550 hPa to ~ 150
130 hPa - illustrating the leading structural characteristic of a jet superposition.

131 Figure 3 shows the frequency of occurrence of vertical jet superposition events over the
132 North Pacific ocean for boreal winters 1979/80 - 2009/10 using the objective identification
133 scheme. It is clear that a maximum in such events resides over the West Pacific within the
134 same region that the near juxtaposition of the tropical and polar tropopauses in the DT57
135 analysis (Fig. 1) is observed. Based upon its being centered on the maximum frequency of
136 occurrence, we consider jet superposition events within the boxed region in Fig. 3.

137 *c. Methodology*

138 To investigate the physical mechanisms associated with the development of vertical jet
139 superpositions in the West Pacific, a composite analysis of robust West Pacific superposition
140 events is performed. The compositing procedure starts by identifying 6-hourly times in which
141 superpositions occur in the boxed region in Fig. 3 ($30 - 40^\circ\text{N}$, $135 - 175^\circ\text{E}$). A robust vertical
142 superposition event is identified if the following criteria are satisfied: 1) at least 7 vertical
143 jet superposition identifications (ID's) occur simultaneously within the interest region, 2)
144 during the 6-hourly time period before superposition, fewer ID's occur than at the time
145 of superposition, and 3) during the 6-hourly time period after the time of superposition,

²The threshold value is $0.64 \times 10^{-5} \text{ PVU m}^{-1}$ for both the 315-330K and 340-355K layers.

³Real-time identifications of the PJ, STJ, and jet superpositions using this identification scheme are available at <http://marrella.aos.wisc.edu/JET/jet.html>.

146 no more than the number of ID’s identified at the time of superposition occur within the
 147 box. The choice of a minimum ID threshold of 7 to define “robust” superposition events is
 148 motivated by the fact that such events are above the 99th percentile of all 6-hourly times we
 149 consider (Table 1).

150 After identifying all 6-hourly times meeting the above requirements (Table 2), meteorological
 151 quantities of interest are averaged over all cases identified in this analysis to construct
 152 composite maps of robust West Pacific superposition events. Specifically, we construct com-
 153 posite maps containing either anomalous or standardized anomalous quantities of interest
 154 as follows:

$$X_{std.anom.} = \frac{X_{supj} - X_{climo}}{X_{stdclimo}} \quad (3)$$

155 where $X_{std.anom.}$ is the standardized anomalous variable for a superposition event, X_{supj}
 156 is the variable measured at the point of interest at the time of the vertical jet superposi-
 157 tion event, X_{climo} is the climatological value of the variable⁴, and $X_{stdclimo}$ is the standard
 158 deviation of the 31-winter climatology of variable X.

159 In the next section, large-scale features associated with superposition events in the West
 160 Pacific are identified via the composite analysis. The evolution of these key features is then
 161 discussed in Section 4.

162 3. Results

163 a. Key Synoptic Features Associated with Composite Vertical Jet Superposition

164 Figure 4 shows various standardized anomalous quantities that characterize the environ-
 165 ment associated with jet superpositions. The composite analysis reveals several key features

⁴The climatological value of X is the 31 winter average (i.e., 1979/80 - 2009/10) of variable X for that specific 6-hourly time in the reanalysis. For example, if a robust superposition occurred on 0000 UTC 14 February 2008, X_{climo} would be the 31 winter average of variable X at 0000 UTC 14 February.

166 that are also present during East Asian Winter Monsoon (EAWM) northerly cold surge
167 events in the West Pacific during boreal winter. The $\vec{v}_{250, std. anom.}$ in Fig. 4a clearly shows
168 a single jet stream entity in the West Pacific, with maximum wind speed in the jet core
169 (located $\sim 160^\circ\text{E}$ longitude) reaching speeds $\geq 90 \text{ m s}^{-1}$. Such speeds in the composite jet
170 core exceed climatology by $> 1.5\sigma$ while flanking anomalies north and south of the jet core
171 are more than 1σ below climatology. This implies that the composite vertically superposed
172 jet is not only faster but also narrower than climatology.

173 Figure 4b shows standardized anomalous geopotential height at 250 hPa ($\phi_{250, std. anom.}$).
174 An anomalous ϕ maximum (minimum) is present on the anticyclonic (cyclonic) shear side
175 of the composite jet. There is also an anomalous ϕ maximum of $\geq 0.5\sigma$ in northern Russia.
176 At 500 hPa (Fig. 4c), an anomalous trough feature resides just to the east of Japan, with
177 $\phi_{500, std. anom.} < -1\sigma$. An anomalous anticyclonic feature in northern Russia exists at this
178 level as well. An anomalous maximum in 500 hPa geopotential height also exists to the
179 southeast of the trough.

180 Figure 4d shows 925 hPa standardized anomalous temperature ($T_{925, std. anom.}$). The combi-
181 nation of anomalous cold air and anomalous northerly wind over the East and South China
182 Sea regions suggests that anomalous cold air advection is occurring there. Anomalous
183 warm temperatures are present on the eastern side of the anomalous anticyclonic flow to the
184 east of the “northerly cold surge” feature.

185 *b. East Asian Winter Monsoon Cold Surges and Jet Superpositions*

186 The EAWM is a boreal winter large-scale circulation phenomenon that is strongly a
187 function of the strength of the Siberian-Mongolian surface high (SMH) pressure system
188 (Chan and Li 2004). The SMH is, in turn, strongly a function of subsidence over the
189 Tibetan plateau and is a “cold” surface phenomena, as it is tied to strong radiative cooling
190 that persists over this region. Northerly cold surge events associated with the SMH occur
191 on its eastern side, as the northerly winds associated with the SMH advect cold air as far

192 south as the South China Sea region, leading to significant cold air outbreak events (Chin
193 1969; Morrice 1973; Chang et al. 1979; Chang and Lau 1980; Chan and Li 2004). Cold
194 surges tied to the EAWM have been extensively investigated over the last several decades,
195 as summarized (for example) in Boyle and Chen (1987) and Chan and Li (2004).

196 A recent study by Wang and Chen (2014) utilizes a seasonal EAWM index based on
197 normalized mean sea level pressure (MSLP) over Siberia, the North Pacific Ocean and the
198 Maritime Continent to determine large-scale features that are associated with strong and
199 weak EAWM winters. In their Figure 3, they showed that strong (weak) EAWM winters
200 are associated with negative (positive) 500 hPa geopotential height anomalies east of Japan,
201 stronger (weaker) 200 hPa zonal winds near the jet entrance region of the West Pacific
202 jet, and anomalous northerly (southerly) wind at 850 hPa. The composite West Pacific
203 jet superposition is also characterized by a strong wind speed along with a minimum in
204 ϕ_{500hPa} over Japan and anomalous northerly winds in the lower troposphere. Other studies
205 such as Jhun and Lee (2004) and Wang and Chen (2010), using other EAWM indices, show
206 that strong EAWM winters are characterized by the presence of similar large-scale features.
207 Additionally, Lee et al. (2010) show that the subtropical Pacific jet is stronger (weaker)
208 during strong (weak) EAWM winters.

209 The studies described above in conjunction with the results of our composite analysis
210 suggest that jet superpositions may be a component of the large-scale circulation associated
211 with EAWM northerly cold surge events. To further explore this possible relationship, the
212 time series of total number of cold season superposition ID's in the box are compared to time
213 series of several EAWM indices used in previous studies (Fig. 5). Four indices are selected
214 from the list of 18 considered by Wang and Chen (2010). We also utilize the EAWM index
215 from Wang and Chen (2014).

216 Figure 5 shows that the time series of the total number of West Pacific superposition
217 ID's is similar to that of the various EAWM indices plotted. For the Jhun and Lee (2004)
218 index (based on 300 hPa zonal wind speed), the number of superposition events increases

219 with increased zonal wind speed. The region where the data was averaged is where the West
220 Pacific jet in boreal winter frequently resides, implying a stronger (weaker) West Pacific
221 jet magnitude during strong (weak) EAWM winters. Since a vertically superposed jet is
222 associated with anomalously higher wind speed (Fig. 4a), the increase (decrease) in jet
223 superposition ID's during strong (weak) EAWM winters is consistent with our composite
224 results.

225 A negative correlation exists between ID counts and the Wang et al. (2009) EAWM index
226 (based on using the first principal component extracted from a principal component analysis
227 on ϕ_{500}), where negative (positive) index values indicate strong (weak) EAWM winters. The
228 correlation implies more (less) jet superposition ID's with lower (higher) geopotential heights
229 in the West Pacific region where mid-tropospheric trough features develop and progress north
230 of the location of the composite jet. Given that an anomalous trough at 500 hPa is observed
231 north of the composite jet (Fig. 4c), the presence of anomalously negative ϕ_{500} values in this
232 region during seasons with more jet superposition events in the West Pacific (Fig. 5) is in
233 line with our results.

234 There is a negative correlation between ID counts and the (Yang et al. 2002) index
235 (based on 850 hPa meridional wind), indicating that a stronger northerly wind is associated
236 with a higher superposition ID frequency of occurrence and vice versa. Stronger northerly
237 (southerly) winds imply a stronger (weaker) cold surge event pattern at 850 hPa and are
238 thus associated with strong (weak) EAWM seasons. Given that a cold anomaly associated
239 with composite anomalous northerly winds is observed in our composite analysis at 925 hPa
240 (Fig. 4a) as well as at 850 hPa (not shown), the Fig. 4d result supports the correlation
241 between jet superposition ID's and the Yang et al. (2002) index.

242 Finally, a positive correlation exists between the MSLP-based indices (i.e., the Chan
243 and Li (2004) and Wang and Chen (2014) indices) and superposition ID counts. Strong
244 (weak) EAWM winters have been shown to be associated with a stronger gradient in MSLP
245 between the Siberian High and Aleutian Low. Since the composite illustrates a strong MSLP

246 gradient between the approximate location of the SMH and Aleutian Low (not shown), the
247 observation of higher (lower) jet superposition ID counts in the West Pacific with a higher
248 (lower) index value is consistent with our composite results.

249 All correlations, except for the Wang et al. (2009) index, are statistically significant
250 at least at the 95% confidence level. The v_{850} and normalized MSLP indices (i.e., Yang
251 et al. (2002) and Wang and Chen (2014), respectively) are both significant at the 99%
252 confidence level. In all cases, the sign of the correlation is such that more vertical jet
253 superposition counts occur during stronger EAWM winters, and vice versa. Based on these
254 simple correlations, we find a robust statistical relationship between the frequency of West
255 Pacific superposition events and the strength of the EAWM.

256 *c. Frequency of Occurrence of EAWM-Like Features from Composite Maps*

257 One of the disadvantages of performing a composite analysis is that large-scale synoptic
258 features prominent within individual cases may be “smoothed out” within composite results.
259 Similarly, large magnitude features appearing in only a few cases (or even a single case) can
260 exact an undue influence in the resulting composite. In order to minimize any associated
261 misinterpretation of the composite results, the number of times at which, for each grid point,
262 values of the standardized variables in Fig. 4 were greater than or less than 0.5σ from the
263 mean were determined. That number was converted to a percentage of the 44 events in the
264 composite. The results of this analysis are shown in Fig. 6.

265 Figure 6a shows that within the core of the composite jet (Fig. 4a), $\geq 90\%$ of the super-
266 position events have $|\vec{u}_{250, std. anom.}| \geq 0.5\sigma$, with $\geq 70\%$ of cases exhibiting $|\vec{u}_{250, std. anom.}| \leq$
267 -0.5σ in the flanking regions of reduced wind speed illustrated in Fig. 4a. Figure 6b shows
268 that for $\geq 50\%$ of superposition cases, many of the grid points on the anticyclonic shear side
269 of the composite jet are associated with $\phi_{250, std. anom.} \geq 0.5\sigma$. At the center of this feature,
270 $\geq 80\%$ of cases meet this criterion. The minimum in $\phi_{250, std. anom.}$ ($\leq -0.5\sigma$) near Japan is
271 equally present in as many as 70 – 80% of cases. Within the region where the composite

272 trough feature at 500 hPa is present, $\phi_{500hPa} \leq -0.5\sigma$ for $\geq 80 - 90\%$ of superposition cases
 273 (Fig. 6c). This feature is present more consistently relative to the upper-tropospheric ridge
 274 and trough features indicated by $\phi_{250,std.anom.}$ in Fig. 6b. Interestingly, the anomalous
 275 geopotential height feature in the mid- to upper troposphere over northern Russia is only
 276 present within $\geq 50 - 60\%$ of the cases within a very localized region northeast (east) of
 277 Lake Baikal at 250 hPa (500 hPa).

278 As for the lower tropospheric “northerly cold surge” feature, Fig. 6d shows that in the
 279 East and South China Sea regions, $T_{925hPa} \leq -0.5\sigma$ for $\geq 80 - 90\%$ of the superposition
 280 cases. Furthermore, the frequency of occurrence of $v_{925,std.anom.}$ in this region is $\leq -0.5\sigma$ for
 281 $\geq 50 - 80\%$ of cases or greater (not shown). Thus, it is clear that the features highlighted in
 282 Fig. 4 are not only associated with strong EAWM winters and related cold surge events, but
 283 also are quite common elements of the 44 cases that comprise the composite jet superposition
 284 (Fig. 6). Accordingly, we conclude that the majority of cases constituting the composite are
 285 associated with some sort of cold surge feature east off the coast of China.

286 *d. Composite Cross Section Results*

287 The compositing methodology is next extended to the construction of composite cross-
 288 sections that illuminate the vertical structure associated with West Pacific jet composite
 289 superposition. Figure 7 shows both the climatological (Fig. 7a) and the superposition
 290 composite (Fig. 7b) vertical cross section along $155^\circ E$ (line C-C' in Fig. 4a) approximately
 291 through the composite jet core. It is clear that the composite superposition is characterized
 292 by a “two-step” tropopause, with a deep tropopause wall stretching from ~ 500 to 150 hPa
 293 and a jet core at ~ 250 hPa. The poleward tilt with height exhibited by the superposed jet
 294 (relative to the climatological jet) is associated with its much larger, and poleward tilted,
 295 horizontal temperature gradient in accord with thermal wind balance.

296 Note that the PV “wall” is much stronger in magnitude (i.e., $|\nabla PV|$) and more vertically
 297 oriented in the composite superposition environment, as indicated by the region of negative

298 (positive) anomalous PV located both equatorward (poleward) of and above (below) the
299 composite jet core (Fig. 7b). The decrease (increase) in PV relative to climatology is associ-
300 ated with anomalously weak (strong) static stability on the equatorward (poleward) side of
301 the composite jet within the STJ (PJ) isentropic layer (i.e., 340-355K and 315-330K, respec-
302 tively). Finally, the jet core has a stronger wind speed maximum in the superposed composite
303 than the climatology; this along with the enhanced “PV wall” are features characteristic of
304 a vertical jet superposition (Fig. 3).

305 Since vertical jet superposition events in the West Pacific appear to be associated with
306 strong EAWM winters and cold surges, cross sections of the composite jet entrance region
307 circulation (120°E longitude) were considered in order to determine whether or not the jet
308 entrance region circulation is enhanced (Fig. 8). The analysis is motivated by observational
309 studies such as Chang et al. (1979), Chang and Lau (1980), Wu and Chan (1997) and Yen and
310 Chen (2002) that show an enhancement of the West Pacific jet as well as the “local Hadley
311 Cell circulation” spanning the Maritime Continent and East China regions during EAWM
312 cold surge events. An enhanced jet entrance region circulation should be characterized
313 by enhanced rising (sinking) motions equatorward (poleward) of the composite jet, with
314 enhanced upper-tropospheric divergence (convergence) and vice versa at the surface.

315 Figure 8a shows anomalous divergence (convergence) in the upper troposphere equator-
316 ward (poleward) of the composite jet. Near the surface below each of these anomalies, the
317 reverse occurs, with anomalous convergence (divergence) equatorward (near or poleward) of
318 the jet. In fact, the anomalous jet entrance region circulation is displaced such that sub-
319 sidence occurs beneath the jet core. Via mass continuity, anomalous upward (downward)
320 vertical motion is present in the air column equatorward of (within) the jet core (Fig. 8b),
321 representing an anomalous enhancement of the jet entrance region circulation.

322 While the analysis thus far reveals that the composite possesses the structural and dy-
323 namical characteristics of a superposed jet, nothing has been shown regarding the evolution
324 of the environment that eventually produces such a jet. These issues are examined in the

325 next section.

326 4. Lagged Composite Map Analysis of West Pacific Ver- 327 tical Jet Superposition

328 a. Evolution of Large-Scale Features Associated with Composite West Pacific Superposition

329 To further investigate the physical mechanisms involved in the production of West Pacific
330 jet superpositions, we construct composite maps at a series of times prior to the time of
331 superposition (Figs. 9-11). At T-3 days, (T=0 is the day of jet superposition), the core of
332 the West Pacific jet resides just south of Japan, with maximum 250 hPa wind speeds over
333 70 m s^{-1} (Fig. 9a). Unlike the composite shown in Fig. 4a, the anomalous flow on the
334 anticyclonic shear side of the composite jet in Fig. 9a is near zero. However, an anomalous
335 upper tropospheric anticyclone with $\phi_{250, std. anom.} > 0.5\sigma$ is present near the right jet entrance
336 region of the composite jet while a minimum in $\phi_{250, std. anom.}$ is present on the cyclonic shear
337 side of the jet. There is also a region of $\phi_{250, std. anom.} > 0.5\sigma$ in northern Russia associated
338 with anomalous anticyclonic flow.

339 At 500 hPa at this time (Fig. 9b), an anomalous trough-like feature is centered near Korea
340 with $\phi_{500, std. anom.} < -0.5\sigma$. A weak anomalous anticyclonic feature near the jet entrance region
341 is also present, and the anomalous anticyclone observed in northern Russia at 250 hPa also
342 exhibits a magnitude $> 0.5\sigma$ at 500 hPa. At 925 hPa (Fig. 9c), anomalous cyclonic flow
343 near Korea and Japan suggest (along with Figs. 9a and 9b) the barotropic nature of the
344 trough feature at this time. Anomalous cold air associated with strong anomalous northerly
345 winds west of Korea along with weaker anomalous northerly winds over the South China Sea
346 are also evident. Note that anomalous anticyclonic flow is also present in northern Russia,
347 suggesting that this feature is approximately barotropic in nature. Finally, Fig. 9d shows
348 anomalous negative OLR values over the Maritime Continent, with the strongest values (in

349 magnitude) confined to $\sim 10^\circ\text{N}$, 130°E . To first order, negative OLR anomalies indicate
350 regions of high cloud tops, likely resulting from composite anomalous convection.

351 By T-2 days, the magnitude of the West Pacific jet has intensified with its core now
352 centered east of southern Japan (Fig. 10a). The $\phi_{250, std. anom.}$ minimum along the cyclonic
353 shear side of the composite jet has strengthened by this time, contributing to the enhance-
354 ment of the composite jet speed. The composite trough at 500 hPa (Fig. 10b) has remained
355 stationary while also intensifying. The anticyclonic flow southwest of the trough observed in
356 Figs. 10a and 10b also remains stationary. The anomalous anticyclone in northern Russia
357 in the middle to upper troposphere moves eastward and strengthens.

358 The anomalous cold air and northerly winds associated with the composite cold surge
359 over eastern China (Fig. 10c) have increased in magnitude while progressing southward
360 at time T-2 days. Attendant with the advance of the cold air, the near-surface anomalous
361 northerly winds at this time extend southward from the East China Sea towards the equator,
362 leading to an increase in near-surface anomalous convergence (not shown). This convergence,
363 in turn, contributes to forcing of anomalous upward vertical motion and the sustenance of
364 anomalous convection in the lower latitudes (Fig. 10d).

365 Finally, by T-1 day, the composite jet is even stronger with jet core wind speeds ex-
366 ceeding 90 m s^{-1} (Fig. 11a). A $\phi_{250, std. anom.}$ maximum that is not discernible to the south
367 of the jet core at T-2 days has grown in strength and areal coverage by this time. The
368 composite $\phi_{250, std. anom.}$ minimum near Japan continues its slow eastward propagation, while
369 the $\phi_{250, std. anom.}$ maximum in northern Russia shifts slightly southward and weakens. The
370 anomalous trough feature at 500 hPa (i.e., $\phi_{500, std. anom.}$ minimum) continues to move east-
371 ward as well while the $\phi_{500, std. anom.}$ maximum in northern Russia evolves in a similar fashion
372 as that observed at 250 hPa.

373 At 925 hPa, the composite cold surge feature and associated anomalous northerly winds
374 continue to move equatorward as the anomalous cyclonic feature east of Japan continues to
375 strengthen (Fig. 11c). The continued equatorward migration of cold air continues to fuel

376 near-surface anomalous convergence which maintains anomalous upward vertical motion and
377 the associated convection in the lower latitudes (Fig. 11d). Note that this convection also
378 spreads poleward at this time. The resulting enhancement of the rising branch of the local
379 meridional overturning circulation plays a role in enhancing the entire composite jet entrance
380 region circulation over the West Pacific, as observed in Fig. 8b.

381 *b. Evolution of Deep, Vertical PV Wall Associated with Composite Jet*

382 While Figs. 9-11 provide some insight regarding the evolution of the key synoptic features
383 in the composites, they offer little explanation of how the deep PV wall structure associated
384 with a negative (positive) PV anomaly on the anticyclonic (cyclonic) shear side of the com-
385 posite jet develops. In this subsection, we investigate the physical mechanisms that reduce
386 (increase) the magnitude of PV equatorward (poleward) of the jet.

387 First, to better understand the mechanisms responsible for the reduction in Ertel PV
388 on the equatorward side of the composite superposed jet, we compute anomalous isentropic
389 pressure depth within the 340-355K isentropic layer, which houses the STJ. Figures 12
390 and 13 show plots of anomalous potential vorticity and anomalous pressure depth within
391 the STJ isentropic layer, respectively, with the panels ordered from T-3 days to composite
392 superposition $T = 0$. Also plotted are the composite 1, 2 and 3 PVU contours as a guide to
393 the tropopause location relative to the anomalous features of interest.

394 Figure 12 shows a negative PV anomaly that develops on the anticyclonic shear side
395 of the composite jet core over the time period. Associated with this feature is a positive
396 pressure depth anomaly (Fig. 13), which also propagates eastward and strengthens over time.
397 The negative PV anomaly at T-3 days (Fig. 12a) elongates and stretches eastward along the
398 equatorward edge of the jet by T-2 days (Fig. 12b). Subsequently, this feature becomes more
399 intense and slightly more isotropic by T-1 day (Fig. 12c) - a trend that continues through to
400 the time of jet superposition (Fig. 12d). The singular negative PV anomaly becomes more
401 negative throughout the 72 hour period in association with an increase in magnitude of the

402 positive pressure depth anomaly (Fig. 13).

403 The presence of the pressure depth anomaly equatorward of the composite jet has two
404 effects on the composite jet core that play a significant role in inducing vertical jet superpo-
405 sition. First, increasing the pressure depth within the STJ layer on the anticyclonic shear
406 side of the composite jet enhances the anomalous anticyclonic flow in that layer in accord
407 with the isentropic thermal wind equation:

$$\frac{\partial \vec{v}_g}{\partial \theta} = \frac{1}{f\rho\theta} \vec{k} \times \nabla p \quad (4)$$

408 where ρ is the density of air. Thus, the expansion and intensification of the pressure depth
409 anomaly on the equatorward side of the jet seen in Fig. 13 is associated with an anomalous
410 anticyclonic vertical geostrophic wind shear that contributes to the anomalous wind speed
411 in the jet core.

412 Secondly, the coincidence of the negative PV anomalies in Fig. 12 with the positive
413 perturbation pressure depths in Fig. 13 may be a function of the fact that the air that fills
414 the STJ layer originates in the tropical/subtropical boundary layer where θ_e is large and PV
415 is small. To illustrate this connection, we adopt a Lagrangian perspective and investigate
416 air parcel back-trajectories generated using the Air Resources Laboratory (ARL) Hybrid
417 Single Particle Lagrangian Integrated Trajectory (HYSPLIT) model (Draxler and Hess 1997,
418 1998; Draxler 1999; Draxler and Rolph 2015; Rolph 2015). Specifically, we compute back-
419 trajectories from the location of the center of the positive pressure depth anomaly maximum
420 at the time of composite superposition (Fig. 13d) for all robust superposition cases we
421 consider.

422 The results of this analysis are shown in Fig. 14, which shows single air parcel back-
423 trajectories in plan view for each case calculated starting at 32.5°N, 160°E. Parcel trajectories
424 starting at altitudes of 10 and 12 km are shown in blue and red, respectively. Figure 14b
425 shows the potential temperature (θ) associated with each trajectory, and Fig. 14c the altitude
426 associated with each parcel over a 120-hour period. It is clear that the majority of the

427 air parcels came from lower latitudes within the vicinity of the negative anomalous OLR
428 observed in Figs. 9d, 10d and 11d, with a few back-trajectories extending westward past the
429 prime meridian. Nearly all of the parcels remain within the middle to upper troposphere
430 between T-5 days and T=0 days (Fig. 14c), tracing the anomalous anticyclonic flow observed
431 in this region (Figs. 4a and 4b). The θ -values associated with these trajectories (Fig.
432 14b) demonstrate that the majority of air parcels remain within the STJ layer throughout
433 the period. Several of these air parcels increased their θ value diabatically over time and
434 ultimately ended up within the STJ layer (Figs. 14b and 14c).

435 The location of many of these parcels over the anomalous negative OLR suggests that
436 upper tropospheric exhaust from convection in the South China Sea may play a role in
437 systematically exporting tropical boundary layer air upward. The anomalous anticyclonic
438 flow present equatorward of the jet then transports this high- θ_e , low-PV air poleward and
439 eastward into the STJ layer on the anticyclonic shear side of the West Pacific jet. This process
440 results not only in an enhancement of the jet core wind speed (via anomalous geostrophic
441 vertical shear associated with the deposition of mass on the south side of the jet), but
442 also accounts for the importation of the negative PV anomaly on that side of the jet that
443 contributes to steepening the PV wall characteristic of a superposed jet.

444 On the poleward side of the jet, a positive PV anomaly within the PJ isentropic layer
445 (associated with the upper tropospheric anomalous trough) propagates eastward over the 72
446 hour period (Fig. 15). At the time of superposition, the positive PV anomaly resides on the
447 poleward side of the composite jet to the northwest of the composite negative PV anomaly
448 within the STJ layer. This feature is responsible for the positive PV anomaly observed in
449 Fig. 7b, and therefore also plays a role in strengthening the PV wall associated with the
450 superposed jet.

451 Recall from Fig. 8b that the jet entrance region circulation associated with the composite
452 superposed jet is both anomalously strong and shifted equatorward. This equatorward shift
453 places the region of anomalous subsidence directly beneath the composite jet core. Such a

454 distribution promotes downward extrusion of stratospheric air into the upper troposphere
455 and is dynamically related to the presence of geostrophic cold air advection in cyclonic shear
456 (e.g., Eliassen 1962; Shapiro 1982; Keyser and Pecnick 1985; Martin 2014).

457 Figure 16 shows composite geostrophic temperature advection and vertical motion at 300
458 hPa (the isobaric level at which the PJ approximately resides) at times T-3, T-2 and T-1
459 prior to composite jet superposition (Figs. 16a, 16b and 16c respectively) as well as at time
460 $T = 0$ (Fig. 16d). It is clear that geostrophic cold air advection is present on the cyclonic
461 shear side of the composite jet entrance region and that the regions of composite cold air
462 advection are associated with composite subsidence. This subsidence, acting throughout the
463 entire 72-hour period prior to superposition, drags high-PV air downward from the lower
464 stratosphere on the poleward side of the jet along the sloping isentropic surfaces within
465 the region of maximum anomalous subsidence shown in Fig. 8b. This process plays a
466 central role in creating the anomalous positive PV feature found on the poleward side of
467 the composite superposed jet (Fig. 7b). Thus, the juxtaposition of opposing PV anomalies
468 across the composite superposed jet (portrayed in Fig. 7b) is a result of internal jet dynamics
469 lowering the polar tropopause on its cyclonic shear side acting in concert with a raising of the
470 subtropical tropopause on its anticyclonic shear side through transport of low-PV, high- θ_e
471 air into the STJ layer.

472 5. Discussion and Conclusions

473 In this paper, an investigation of the structure and evolution of the large-scale features
474 most commonly associated with wintertime vertical jet superposition events in the West
475 Pacific has been presented. The study focused on composite analysis of 44 particularly
476 robust superposition events observed over 31 winters using the NCEP/NCAR Reanalysis 1
477 Dataset.

478 The analysis reveals that the most robust synoptic features associated with West Pacific

479 jet superposition events are: 1) A single, strong and latitudinally narrow composite West
480 Pacific jet stream with a wind speed maximum of $\geq 90 \text{ m s}^{-1}$, 2) a positive/negative couplet
481 of $\phi_{250, \text{std. anom.}}$ anomaly straddling the composite West Pacific jet, 3) an anomalous trough
482 ($\phi_{500, \text{std. anom.}}$ minimum) on the cyclonic shear side of the composite jet and 4) a negative
483 $T_{925, \text{std. anom.}}$ feature that resembles a “cold surge” type of event that occurs during strong
484 EAWM winters (Fig. 4). All of these features are shown to occur within the majority of the
485 superposition events selected for the analysis (Fig. 6).

486 The simultaneous presence of a strong jet along with middle tropospheric trough and
487 cold surge anomalies are also characteristic features of EAWM cold surge events, suggesting
488 that West Pacific jet superposition events may be preferentially tied to the cold surges of
489 strong EAWM winters. Statistical support for this suggestion arises from the fact that
490 several EAWM indices are significantly correlated with the number of jet superposition ID’s
491 that occur in the West Pacific analysis region (Fig. 5). Future work will include further
492 exploration of this suggested relationship.

493 Cross sections through the composite jet core (Fig. 7) show a two-step tropopause and
494 a deep PV wall through the jet; both the stronger winds and deeper PV wall relative to
495 climatology are features characteristic of West Pacific jet superpositions (Fig. 3d). Also,
496 negative (positive) anomalous Ertel PV equatorward (poleward) of the jet core is present
497 (Fig. 7b) associated with weak (strong) static stability within the STJ isentropic layer (Fig.
498 7b). The jet entrance region circulation associated with the composite superposed jet is also
499 stronger relative to climatology (Fig. 8), and is shifted equatorward such that subsidence
500 occurs beneath the jet core in its entrance region.

501 To better understand the evolution of key synoptic features that lead to robust West
502 Pacific jet superposition, composite maps at times 1-3 days prior to composite jet superpo-
503 sition were constructed. The relationship between these key features and their respective
504 evolutions is summarized in a conceptual model illustrated in Fig. 17. A near surface cold
505 air anomaly is located in northeastern China 3 days prior to composite jet superposition

506 (Fig. 17a). Anomalous convection in the tropical West Pacific (cloud symbols in Fig. 17a)
507 is also present. As the cold pool moves equatorward over time, the associated anomalous
508 northerly winds (purple arrows in Fig. 17) increase anomalous near-surface convergence in
509 the tropical West Pacific, which fuels anomalous upward vertical motions (dot over the cloud
510 symbols in Fig. 17b) that, in turn, sustain pre-existing anomalous convection. This leads
511 to anomalous divergence aloft (red shaded oval with black dot in center in Fig. 17b). An
512 attendant region of anomalous convergence aloft poleward and above the region of cold air
513 is also present, associated with anomalous subsidence via mass continuity (blue circle with
514 “X” in Fig. 17b).

515 High- θ_e , low-PV convective outflow on the equatorward side of the jet is advected by
516 the anomalous anticyclonic flow east of the anomalous convection (brown arrows with “H”
517 in Fig. 17c). Given that this air has $\theta_e \approx 350$ K, as it is advected poleward, it is locally
518 exhausted within the STJ isentropic layer on the equatorward side of the composite jet (jet
519 symbol with black contour in Fig. 17c). The movement of this air into the STJ layer on
520 the anticyclonic shear side of the jet increases the anomalous pressure depth. This not only
521 induces anomalous anticyclonic shear equatorward of the jet, enhancing the anomalous wind
522 speed within the jet core, but also acts to reduce the PV on the equatorward side of the
523 jet core such that the PV gradient (i.e., in the 1-3 PVU channel) associated with the jet
524 becomes stronger and more vertically oriented (Fig. 17d).

525 On the cyclonic shear side of the composite jet, geostrophic cold air advection in cyclonic
526 shear drives subsidence through the jet core in its entrance region, transporting high-PV air
527 downward and thus increasing the strength of the positive PV anomaly poleward of the jet
528 core (Figs. 15 and 16). This positive PV anomaly plays a role in increasing the magnitude of
529 the 1-3 PVU gradient as well as in shaping the PV wall into a more vertical orientation. The
530 increase in anomalous wind speed coincident with the development of a deep and vertical
531 PV wall are the hallmarks of a West Pacific vertical jet superposition.

532 This conceptual model shows many elements of the various conceptual models and results

533 from Chang et al. (1979), Chang and Lau (1980) and Wu and Chan (1997). For example,
534 as shown in Figure 14 of Chang and Lau (1980), as cold air on the eastern side of the
535 Siberian-Mongolian High (SMH) is advected equatorward, the associated strong northerly
536 winds may lead to enhanced surface convergence in the West Pacific equatorial region. This
537 convergence sustains pre-existing tropical convection in the equatorial West Pacific which, in
538 turn, enhances the local Hadley cell circulation (Chang and Lau 1980; Wu and Chan 1997).
539 Enhanced poleward flow associated with the invigorated Hadley cell induces a stronger West
540 Pacific jet via enhanced angular momentum transport.

541 In Chang et al. (1979) and Chang and Lau (1980), it was shown that EAWM cold surge
542 events induce enhanced surface convergence in the West Pacific equatorial region, which
543 helps to intensify the local Hadley Cell circulation in the region and subsequently enhance
544 the speed of the West Pacific jet. While the present analysis shows an enhancement of the
545 jet in this region associated with the presence of a cold surge, it appears in our conceptual
546 model as a component of the larger scale evolution of an environment that produces a vertical
547 superposition of the usually separate polar and subtropical jets. Those physical mechanisms
548 associated with EAWM cold surges that strengthen the West Pacific jet appear to be vital
549 elements in the development of West Pacific superposition events.

550 It is interesting to note that even within the climatological cross section through the jet
551 core (Fig. 7a), only two steps in the tropopause are evident, implying that the West Pacific
552 jet borders on a superposed structure rather frequently as suggested by Christenson (2013).
553 The foregoing analysis, however, makes clear that, despite the temptation to consider the
554 West Pacific jet as a single monolithic feature, only the correct collection of circumstances
555 can foster production of the relatively rare vertical jet superposition. It appears that cold
556 surge events, associated as they are with an increase in the strength of the West Pacific jet
557 entrance region circulation, the transport of high θ_e , low-PV air into the STJ isentropic layer
558 and the occurrence of geostrophic cold air advection in cyclonic shear in the jet entrance
559 region, are key physical mechanisms that help to induce robust vertical jet superposition.

560 A number of additional research questions remain to be explored in the wake of the
561 foregoing analysis. For example, although several of the air parcel trajectories in Fig. 14
562 trace back to the region of negative anomalous OLR near Indonesia, further trajectory
563 analysis is required to investigate the percentage of cases in which the low-PV, high- θ_e air
564 on the equatorward flank of the superposed jet core is transported upward directly from the
565 tropical boundary layer.

566 The cold surges in our composite results play a key role in producing jet superpositions.
567 Therefore, understanding the mechanisms triggering these cold surge events would further
568 illuminate our conception of the life cycle of West Pacific jet superpositions. For example,
569 it has been shown that cold surges in East Asia can result from the propagation of a Rossby
570 wave train from central Eurasia southeastward, noted as a wave train of “Atlantic origin”
571 (Takaya and Nakamura 2005). We suggest that repeating our composite analysis for days
572 prior to T-3 would lend additional insight into the development of cold surges.

573 It would also be beneficial to investigate the downstream effects of West Pacific jet su-
574 perpositions on weather events throughout the Northern Hemisphere. This topic can be
575 investigated using the same composite analysis technique we use in our methodology, inves-
576 tigating times up to several days after composite jet superposition (i.e., composite analysis
577 at times T+1, T+2, ..., T+5 days). Such an analysis would provide further understanding
578 of any relationship that these events have with other large-scale Northern Hemisphere tele-
579 connections and thus support improved understanding and prediction of significant weather
580 events that derive from West Pacific jet superpositions. Finally, given the significant corre-
581 lation between various EAWM indices and the number of jet superposition ID’s in our West
582 Pacific interest region, it is of interest to compare and contrast the physical processes leading
583 to jet superposition within strong versus weak EAWM seasons. Such analyses are currently
584 ongoing.

585 *Acknowledgments.*

586 We thank the two anonymous reviewers for their constructive feedback. We also thank
587 Rich Pawlowicz for making the “M_Map” MATLAB mapping package available for public
588 use for plotting high resolution continental borders. This work is funded by the National
589 Science Foundation through grant AGS-1265182.

REFERENCES

- 592 Bosart, L. F., G. J. Hakim, K. R. Tyle, M. A. Bedrick, W. E. Bracken, M. J. Dickinson,
593 and D. M. Schultz, 1996: Large-Scale Antecedent Conditions Associated with the 12-14
594 March 1993 Cyclone (“Superstorm ’93”) over Eastern North America. *Mon. Wea. Rev.*,
595 **124**, 1865–1891.
- 596 Boyle, J. S., and T.-J. Chen, 1987: Synoptic Aspects of the Wintertime East Asian Monsoon.
597 *Monsoon Meteorology*, C.-P. Chang, and T. N. Krishnamurti, Eds., Oxford University
598 Press, 125–160.
- 599 Chan, J. C. L., and C. Y. Li, 2004: The East Asian Winter Monsoon. *The Asian Monsoon*,
600 C. Chang, Ed., World Scientific, 54–106.
- 601 Chang, C.-P., J. Erickson, and K.-M. Lau, 1979: Northeasterly Cold Surges and Near-
602 Equatorial Disturbances over the Winter-MONEX Area during 1974. Part 1: Synoptic
603 Aspects. *Mon. Wea. Rev.*, **107**, 812–829.
- 604 Chang, C.-P., and K.-M. Lau, 1980: Northeasterly Cold Surges and Near-Equatorial Dis-
605 turbances over the Winter-MONEX Area during 1974. Part 2: Planetary-Scale Aspects.
606 *Mon. Wea. Rev.*, **108**, 298–312.
- 607 Chin, P., 1969: Cold Surges over South China. Tech. rep., Tech. Note No. 28, Royal Obser-
608 vatory Hong Kong, 40 pp.
- 609 Christenson, C. E., 2013: A Synoptic-Climatology of Northern Hemisphere Polar and Sub-
610 tropical Jet Superposition Events. M.S. thesis, Department of Atmospheric and Oceanic
611 Sciences, University of Wisconsin - Madison, 62 pp.

- 612 Cunningham, P., and D. Keyser, 2004: Dynamics of Jet Streaks in a Stratified Quasi-
613 Geostrophic Atmosphere: Steady-State Representations. *Quart. J. Roy. Meteor. Soc.*, **130**,
614 1579–1609.
- 615 Defant, F., and H. Taba, 1957: The Threefold Structure of the Atmosphere and the Char-
616 acteristics of the Tropopause. *Tellus*, **9**, 259–275.
- 617 Draxler, R. R., 1999: HYSPLIT4 User’s Guide. NOAA Tech. Memo. Tech. rep., ERL ARL-
618 230, NOAA Air Resources Laboratory, Silver Spring, MD.
- 619 Draxler, R. R., and G. D. Hess, 1997: Description of the HYSPLIT_4 Modeling System.
620 NOAA Tech. Memo. Tech. rep., ERL ARL-224, NOAA Air Resources Laboratory, Silver
621 Spring, MD, 24 pp.
- 622 Draxler, R. R., and G. D. Hess, 1998: An Overview of the HYSPLIT_4 Modeling System of
623 Trajectories, Dispersion, and Deposition. *Aust. Meteor. Mag.*, **47**, 295–308.
- 624 Draxler, R. R., and G. D. Rolph, 2015: HYSPLIT (HYbrid Single-Particle La-
625 grangian Integrated Trajectory) Model Access via NOAA ARL READY Website
626 (<http://ready.arl.noaa.gov/HYSPLIT.php>). NOAA Air Resources Laboratory, Silver
627 Spring, MD.
- 628 Eliassen, A., 1962: On the Vertical Circulation in Frontal Zones. *Geophys. Publ.*, **24**, 147–
629 160.
- 630 Hakim, G. J., D. Keyser, and L. F. Bosart, 1996: The Ohio Valley Wave Merger Cyclogenesis
631 Event of 25-26 January 1978. Part II: Diagnosis using Quasigeostrophic Potential Vorticity
632 Inversion. *Mon. Wea. Rev.*, **124**, 2176–2205.
- 633 Hoskins, B. J., and P. Berrisford, 1988: A Potential Vorticity Perspective of the Storm of
634 15-16 October 1987. *Weather*, **43**, 122–129.

- 635 Jhun, J. G., and E. J. Lee, 2004: A New East Asian Winter Monsoon Index and associated
636 Characteristics of the Winter Monsoon. *J. Climate*, **17**, 711–726.
- 637 Kalnay, E., and Coauthors, 1996: The NCEP/NCAR 40-Year Reanalysis Project. *Bull.*
638 *Amer. Meteor. Soc.*, **77**, 437–471.
- 639 Keyser, D., and M. J. Pecnick, 1985: A Two-Dimensional Primitive Equation Model of
640 Frontogenesis forced by Confluence and Horizontal Shear. *J. Atmos. Sci.*, **42**, 1259–1282.
- 641 Keyser, D., and M. A. Shapiro, 1986: A Review of the Structure and Dynamics of Upper-
642 Level Frontal Zones. *Mon. Wea. Rev.*, **114**, 452–499.
- 643 Koetswaram, P., 1953: An Analysis of the High Tropospheric Wind Circulation over India
644 in Winter. *Indian J. Meteor. Geophys.*, **4**, 13–21.
- 645 Koetswaram, P., and S. Parthasarathy, 1954: The Mean Jet Stream over India in the Pre-
646 Monsoon and Post-Monsoon Seasons and Vertical Motions associated with Subtropical
647 Jet Streams. *Indian J. Meteor. Geophys.*, **5**, 138–156.
- 648 Krishnamurti, T. N., 1961: On the Role of the Subtropical Jet Stream of Winter in the
649 Atmospheric General Circulation. *J. Meteor.*, **18**, 657–670.
- 650 Lee, Y.-Y., G.-H. Lim, and J.-S. Kug, 2010: Influence of the East Asian Winter Monsoon
651 on the Storm Track Activity over the North Pacific. *J. Geophys. Res.*, **115**, D09 102.
- 652 Loewe, F., and V. Radok, 1950a: A Meridional Aerological Cross Section in the Southwest
653 Pacific. *J. Meteor.*, **7**, 58–65.
- 654 Loewe, F., and V. Radok, 1950b: Some Amendments to “A Meridional Aerological Cross-
655 Section in the Southwest Pacific. *J. Meteor.*, **7**, 305–306.
- 656 Martin, J. E., 2014: Quasi-Geostrophic Diagnosis of the Influence of Vorticity Advection
657 on the Development of Upper Level Jet-Front Systems. *Q. J. R. Meteorol. Soc.*, **140**,
658 2658–2671.

659 Mohri, K., 1953: On the Fields of Wind and Temperature over Japan and Adjacent Waters
660 during Winter of 1950–1951. *Tellus*, **5**, 340–358.

661 Morrice, A. M., 1973: Quantitative Forecasting of the Winter Monsoon in Hong Kong. Tech.
662 rep., Tech. Note No. 35, Royal Observatory Hong Kong, 41 pp.

663 Namias, J., and P. F. Clapp, 1949: Confluence theory of the high tropospheric jet stream.
664 *J. Meteor.*, **6**, 330–336.

665 Newton, C. W., 1954: Frontogenesis and Frontolysis as a Three-Dimensional Process. *J.*
666 *Meteor.*, **11**, 449–461.

667 Palmén, E., and C. W. Newton, 1969: *Atmospheric Circulation Systems: Their Structure*
668 *and Physical Interpretation*. Academic Press, 603 pp.

669 Reiter, E. R., 1961: *Meteorologie der Strahlströme (Meteorology of the Jet Streams)*.
670 Springer-Verlag, Vienna, 473 pp.

671 Reiter, E. R., 1963: *Jet Stream Meteorology*. University of Chicago Press, 515 pp.

672 Reiter, E. R., and L. F. Whitney, 1969: Interaction between Subtropical and Polar-Front
673 Jet Stream. *Mon. Wea. Rev.*, **97**, 432–438.

674 Riehl, H., 1962: Jet Streams of the Atmosphere. Tech. rep., Dept. of Atmospheric Science,
675 Colorado State University Tech. Rep. 32, Fort Collins, Colorado, 117 pp.

676 Rolph, G. D., 2015: Real-time Environmental Applications and Display sYstem (READY)
677 Website (<http://ready.arl.noaa.gov>). NOAA Air Resources Laboratory, Silver Spring, MD.

678 Shapiro, M. A., 1982: Mesoscale Weather Systems of the Central United States. Tech. rep.,
679 CIRES Univ. of Colorado/NOAA: Boulder, CO, 78 pp.

- 680 Shapiro, M. A., and D. Keyser, 1990: Fronts, Jet Streams, and the Tropopause. *Extratropical*
681 *Cyclones: The Erik Palmn Memorial Volume*, C. Newton, and E. O. Holopainen, Eds.,
682 Amer. Meteor. Soc., 167–191.
- 683 Sutcliffe, R. C., and J. K. Bannon, 1954: Seasonal Changes in the Upper-Air Conditions in
684 the Mediterranean Middle East Area. *Scientific Proceedings of the International Associa-*
685 *tion of Meteorology*, Rome, Italy, Int. Union of Geodesy and Geophysics, 322–334.
- 686 Wang, L., and W. Chen, 2010: How Well do Existing Indices Measure the Strength of the
687 East Asian Winter Monsoon? *Adv. Atmos. Sci.*, **27**, 855–870.
- 688 Wang, L., and W. Chen, 2014: An Intensity Index for the East Asian Winter Monsoon. *J.*
689 *Climate*, **27**, 2361–2374.
- 690 Wang, L., W. Chen, W. Zhou, and R. Huang, 2009: Interannual Variations of East Asian
691 Trough Axis at 500 hPa and its Association with the East Asian Winter Monsoon Pathway.
692 *J. Climate*, **22**, 600–614.
- 693 Winters, A. C., and J. E. Martin, 2014: The Role of a Polar/Subtropical Jet Superposition
694 in the May 2010 Nashville Flood. *Wea. Forecasting*, **29**, 954–974.
- 695 Wu, M. C., and J. C. L. Chan, 1997: Upper-level Features Associated with Winter Monsoon
696 Surges over South China. *Mon. Wea. Rev.*, **125**, 317–340.
- 697 Yang, S., K. M. Lau, and K. M. Kim, 2002: Variations of the East Asian Jet Stream and
698 Asian–Pacific–American Winter Climate Anomalies. *J. Climate*, **15**, 306–325.
- 699 Yeh, T. C., 1950: The Circulation of the High Troposphere over China in the Winter of
700 1945-46. *Tellus*, **2**, 173–183.
- 701 Yen, M.-C., and T.-C. Chen, 2002: A Revisit of the Tropical-Midlatitude Interaction in East
702 Asia caused by Cold Surges. *J. Meteor. Soc. Japan*, **80**, 1115–1128.

703 **List of Tables**

704	1	Number of 6-hourly times where “X” number of vertical jet superposition ID’s	
705		are found in the West Pacific region of interest (boxed in Fig. 3), where “X”	
706		is the value in column 1 of this table.	31
707	2	List of 44 robust West Pacific vertical jet superposition events identified using	
708		the methodology described in Section 2c.	32

TABLE 1. Number of 6-hourly times where “X” number of vertical jet superposition ID’s are found in the West Pacific region of interest (boxed in Fig. 3), where “X” is the value in column 1 of this table.

X	Number of Times with X ID’s	Percent of 6-hourly times with X or more ID’s
1	1451	13.0%
2	862	7.72%
3	532	4.77%
4	309	2.77%
5	184	1.65%
6	114	1.02%
7	66	0.591%
8	36	0.323%
9	22	0.197%
10	13	0.117%

TABLE 2. List of 44 robust West Pacific vertical jet superposition events identified using the methodology described in Section 2c.

Robust Event Date/Time	Robust Event Date/Time
07 February 1980 (0000 UTC)	14 February 1999 (1200 UTC)
29 December 1980 (0600 UTC)	23 December 1999 (0000 UTC)
11 January 1981 (0600 UTC)	31 January 2000 (0600 UTC)
29 January 1981 (1200 UTC)	16 February 2000 (1200 UTC)
14 December 1981 (1800 UTC)	17 February 2000 (0000 UTC)
15 December 1981 (1800 UTC)	11 December 2000 (0600 UTC)
04 February 1987 (0600 UTC)	04 January 2001 (0000 UTC)
10 January 1988 (0000 UTC)	04 January 2001 (1200 UTC)
23 February 1991 (1200 UTC)	15 January 2001 (0000 UTC)
24 February 1991 (1800 UTC)	15 January 2001 (1200 UTC)
25 February 1991 (1200 UTC)	16 January 2001 (0000 UTC)
24 February 1993 (1800 UTC)	19 February 2002 (1800 UTC)
25 December 1995 (0000 UTC)	21 December 2003 (0000 UTC)
25 December 1995 (1800 UTC)	26 December 2003 (1800 UTC)
01 February 1996 (0000 UTC)	07 February 2004 (0600 UTC)
02 February 1996 (1200 UTC)	27 December 2005 (1800 UTC)
01 December 1996 (0000 UTC)	10 January 2007 (0000 UTC)
01 December 1996 (1200 UTC)	15 February 2008 (0000 UTC)
02 December 1996 (0000 UTC)	16 February 2008 (0000 UTC)
09 January 1999 (1200 UTC)	16 February 2008 (1800 UTC)
12 January 1999 (1200 UTC)	08 January 2010 (1200 UTC)
13 February 1999 (0000 UTC)	15 January 2010 (1200 UTC)

709 List of Figures

710 1 a) From Winters and Martin (2014), color-enhanced (from DT57) mean merid-
711 ional cross section of isentropic (θ) surfaces (units K, solid black lines) along
712 with labeled jet stream locations (“J” symbols) and the tropical, subtropical
713 and polar tropopause steps (dashed contours, see legend at bottom of figure)
714 on 1 January 1956. The polar frontal zone is also labeled (solid red contour).
715 b) From DT57: Tropopause height (hPa) over the Northern Hemisphere at
716 0300 UTC on 1 January 1956. The yellow regions represent the tropical
717 tropopause height, white regions represent the subtropical tropopause height
718 and red regions represent the polar tropopause height. The PJ (STJ) approx-
719 imately resides along the strong concentrations in isolines bordering between
720 the red and white (yellow and white) regions. 39

721 2 From Winters and Martin (2014): a) 300-hPa isotachs shaded every 10 m s^{-1}
722 starting at 30 m s^{-1} showing separate polar and subtropical jets near the west
723 coast of the U.S. at 0000 UTC 27 April 2010. b) Cross section A-A’ through
724 both the polar and subtropical jet cores from panel a) with 1-, 2-, and 3-PVU
725 surfaces contoured in black, 4-, 5-, 6-, 7-, 8-, and 9-PVU surfaces contoured
726 in light blue, potential temperature contoured every 5 K in dashed green, and
727 isotachs (red) every 10 m s^{-1} starting at 30 m s^{-1} . The PJ and STJ jet cores
728 are shaded in yellow and the 315-330 and 340-355K isentropic layers (i.e., PJ
729 and STJ isentropic layers, respectively), are shaded in grey. The blue (red)
730 lines through a grid column with a black dot represent the identification of a
731 polar (subtropical) jet. c) Same as panel a) but for a vertical jet superposition
732 event at 0000 UTC 24 Oct 2010. d) Same as panel b) but for the cross section
733 B-B’ in panel c), with the PJ and STJ identifications (black dots) occurring
734 within the same grid column indicating a jet superposition. 40

- 735 3 Frequency of occurrence of vertical jet superposition events over the Pacific
736 Ocean in the Northern Hemisphere during boreal winters 1979/80 - 2009/10.
737 The black box region represents the region of interest in our study. 41
- 738 4 Composite maps over the North Pacific ocean. a) $\vec{v}_{250, std. anom.}$ (fill; yellow
739 (blue) colors represent values \geq (\leq) 0.5σ from climatology), b) $\phi_{250, std. anom.}$
740 (same fill pattern conventions as panel a), c) $\phi_{500, std. anom.}$ (same fill pattern
741 conventions as panel a) and d) $T_{925, std. anom.}$ (same fill pattern conventions
742 as panel a). On all maps, anomalous wind speeds at the level specified are
743 plotted as vectors, and composite wind speed at 250 hPa is plotted as solid
744 red contours every 10 m s^{-1} starting at 30 m s^{-1} . All maps are composite
745 at the time of West Pacific vertical jet superposition. The cross section lines
746 C-C' and D-D' are relevant for Figs. 7 and 8, respectively. 42
- 747 5 Time Series of cold season standardized jet superposition ID frequency in the
748 West Pacific box region (thick black solid line) along with 5 standardized
749 EAWM indices for winters 1979/80 - 2009/10. Note that for the Yang et al.
750 (2002) and Wang et al. (2009) time series plots, the time series were mul-
751 tiplied by -1 so that for all indices shown, positive (negative) values imply
752 strong (weak) EAWM winters. Also included are the correlation coefficients
753 between each EAWMI and superposition ID frequency, where values with a
754 single (double) asterisk are significant at the 95% (99%) level (note that we
755 assume each winter season is independent of the others such that the number
756 of degrees of freedom = $N-2$, with $N = 31$). 43
- 757 6 Percent occurrence of each of the standardized variables in Fig. 4 for all
758 44 cases used in the composite. Red (blue) contours indicate regions where
759 variable of interest with standardized value $\geq 0.5\sigma$ ($\leq -0.5\sigma$) occurs in at least
760 50% of cases contoured every 10%. Variables in each panel match those of
761 Fig. 4. 44

762 7 a) Climatological composite cross section taken along 155°E longitude (C-C'
763 line from Fig. 4a) of wind speed (solid red contour; 10 m s⁻¹ intervals starting
764 at 30 m s⁻¹), isentropic surfaces (solid gray contour every 5 K starting at
765 280 K with levels within 315-330 K and 340-355 K layers in thicker black
766 contour, labeled and shaded in light gray) and the 1-3 PVU channel in the
767 upper troposphere (solid blue contour; units PVU). b) Same as Fig. 7a but
768 for the composite superposition data, including anomalous Ertel PV (solid
769 (dashed) green contour every 0.5 PVU starting at + (-) 0.5 PVU). Note that
770 the climatological composite cross section is computed by averaging together
771 the climatological data for all 44 dates/times considered in this study, with the
772 climatology for each date/time being the 31 year average at that particular
773 time. 45

774 8 Cross sections taken along 120°E longitude (D-D' line from Fig. 4a). All
775 conventions are the same as that of Fig. 7 except that the solid (dashed)
776 green contour represents anomalous divergence (convergence) every 0.5 x 10⁻⁶
777 s⁻¹ starting at + (-) 0.5 x 10⁻⁶ s⁻¹ in panel a and the solid (dashed) purple
778 contour represents anomalous downward (upward) vertical motion every 0.01
779 Pa s⁻¹ starting at + (-) 0.01⁻² Pa s⁻¹ in panel b. 46

780 9 Composite maps of a) $\phi_{250, std. anom.}$, b) $\phi_{500, std. anom.}$, c) $T_{925, std. anom.}$ and d)
781 daily-averaged anomalous interpolated Outgoing Longwave Radiation (OLR)
782 3 days prior to composite West Pacific vertical jet superposition. Conventions
783 are the same as Fig. 4 except for the OLR plots, where the anomalous OLR
784 values are contoured every 10 W m⁻² starting at + (-) 10 W m⁻², and wind
785 vectors represent 250 hPa anomalous wind (m s⁻¹). 47

786 10 Same as Fig. 9, but time prior to vertical jet superposition is 2 days rather
787 than 3 days. 48

- 788 11 Same as Fig. 9, but time prior to vertical jet superposition is 1 day rather
789 than 3 days. 49
- 790 12 Anomalous PV (PV units) within the STJ (340-355K) isentropic layer (fill
791 pattern) at a) 3 days prior to composite superposition, b) 2 days prior to
792 composite superposition, c) 1 day prior to composite superposition and d) at
793 the time of composite superposition. The 1-3 PVU surfaces are contoured in
794 solid purple. Anomalous winds within the STJ layer are shown as vectors. 50
- 795 13 Composite anomalous pressure depth within the STJ (340-355K) isentropic
796 layer (fill pattern) at a) 3 days prior to composite superposition, b) 2 days
797 prior to composite superposition, c) 1 day prior to composite superposition
798 and d) at the time of composite superposition. Note that $dp = p_{340K} - p_{355K}$
799 for the 340-355K isentropic layer. 1-3 PVU surfaces are contoured in solid
800 purple. Anomalous winds within the STJ layer are shown as vectors. 51
- 801 14 a) Same as Fig. 13d, but included are ARL HYSPLIT 120 hour back-
802 trajectories for air parcels, where the trajectories begin at the center of the
803 anomalous pressure depth feature within the STJ isentropic layer (32.5°N ,
804 160°E). Trajectories colored in blue (red) represent parcels with back-trajectories
805 starting at 10 km (12 km). b) Time series of θ (K) associated with each par-
806 cel back-trajectory shown in panel a. Color conventions for the time series
807 are same as that of the trajectories from panel a. The STJ isentropic layer
808 lies between the solid black lines (340-355K). c) Time series of altitude (km)
809 associated with each parcel back-trajectory shown in panel a. The color con-
810 ventions are the same as panel b. 52

- 811 15 Anomalous PV (PV units) within the PJ (315-330K) isentropic layer (fill
812 pattern) at a) 3 days prior to composite superposition, b) 2 days prior to
813 composite superposition, c) 1 day prior to composite superposition and d) at
814 the time of composite superposition. The 1-3 PVU surfaces are contoured in
815 solid purple. Anomalous winds within the PJ layer are shown as vectors. 53
- 816 16 300 hPa composite geostrophic temperature advection (fill pattern; units K
817 s^{-1}) and vertical motion (red (purple) solid (dashed) contour indicates upward
818 (downward) vertical motion) contoured every 0.05 Pa s^{-1} starting at + (-)
819 0.05 Pa s^{-1} for times a) 3 days prior to jet superposition, b) 2 days prior to
820 jet superposition, c) 1 day prior to jet superposition, and d) at time of jet
821 superposition. Also plotted on all panels are 300 hPa composite wind speed
822 (black solid contour) every 10 m s^{-1} starting at 30 m s^{-1} . 54

823 17 Conceptual model outlining the role of tropical forcing with respect to onset
824 of robust vertical jet superposition events in the West Pacific. In panel a), the
825 green arrows with the abbreviation “SMH” represents the Siberian-Mongolian
826 High, the purple arrows represent near-surface anomalous northerly winds,
827 the blue cloud symbols represent anomalous tropical convection and the black
828 thin circle with the westerly vector represents the approximate position of the
829 composite jet. All features in panel a) are present 3 days prior to composite
830 vertical jet superposition. In panel b), the blue (red) circle indicates the
831 region of anomalous upper tropospheric convergence (divergence), with the
832 “x” (dot) symbol representing anomalous downward (upward) vertical motion
833 within the air column. In panel c), the brown arrows with the “H” in the
834 center represents the anomalous geopotential height maximum feature on the
835 anticyclonic shear side of the jet that develops 48 hours prior to composite jet
836 superposition. The hatched green arrow represents the direction of transport
837 of high- θ_e , low-PV air mass from the tropics towards the region where the
838 anomalous anticyclone develops equatorward of the jet. Panel d) demonstrates
839 the role of low-PV, high- θ_e air associated with tropical convective outflow as
840 it is transported into the STJ isentropic layer equatorward of the superposed
841 jet. The orange arrow represents subsidence within the jet entrance region
842 that plays a role in the development of the deep, vertical PV wall associated
843 with the composite superposed jet. See text for further explanation.

55

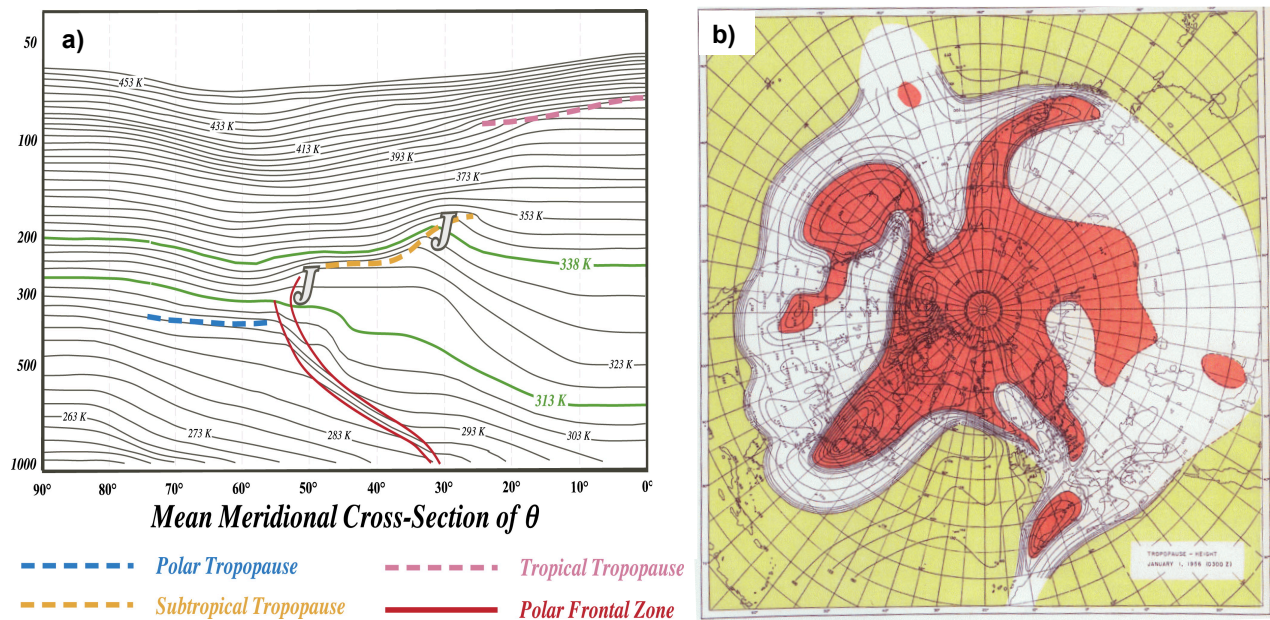


FIG. 1. a) From Winters and Martin (2014), color-enhanced (from DT57) mean meridional cross section of isentropic (θ) surfaces (units K, solid black lines) along with labeled jet stream locations (“J” symbols) and the tropical, subtropical and polar tropopause steps (dashed contours, see legend at bottom of figure) on 1 January 1956. The polar frontal zone is also labeled (solid red contour). b) From DT57: Tropopause height (hPa) over the Northern Hemisphere at 0300 UTC on 1 January 1956. The yellow regions represent the tropical tropopause height, white regions represent the subtropical tropopause height and red regions represent the polar tropopause height. The PJ (STJ) approximately resides along the strong concentrations in isolines bordering between the red and white (yellow and white) regions.

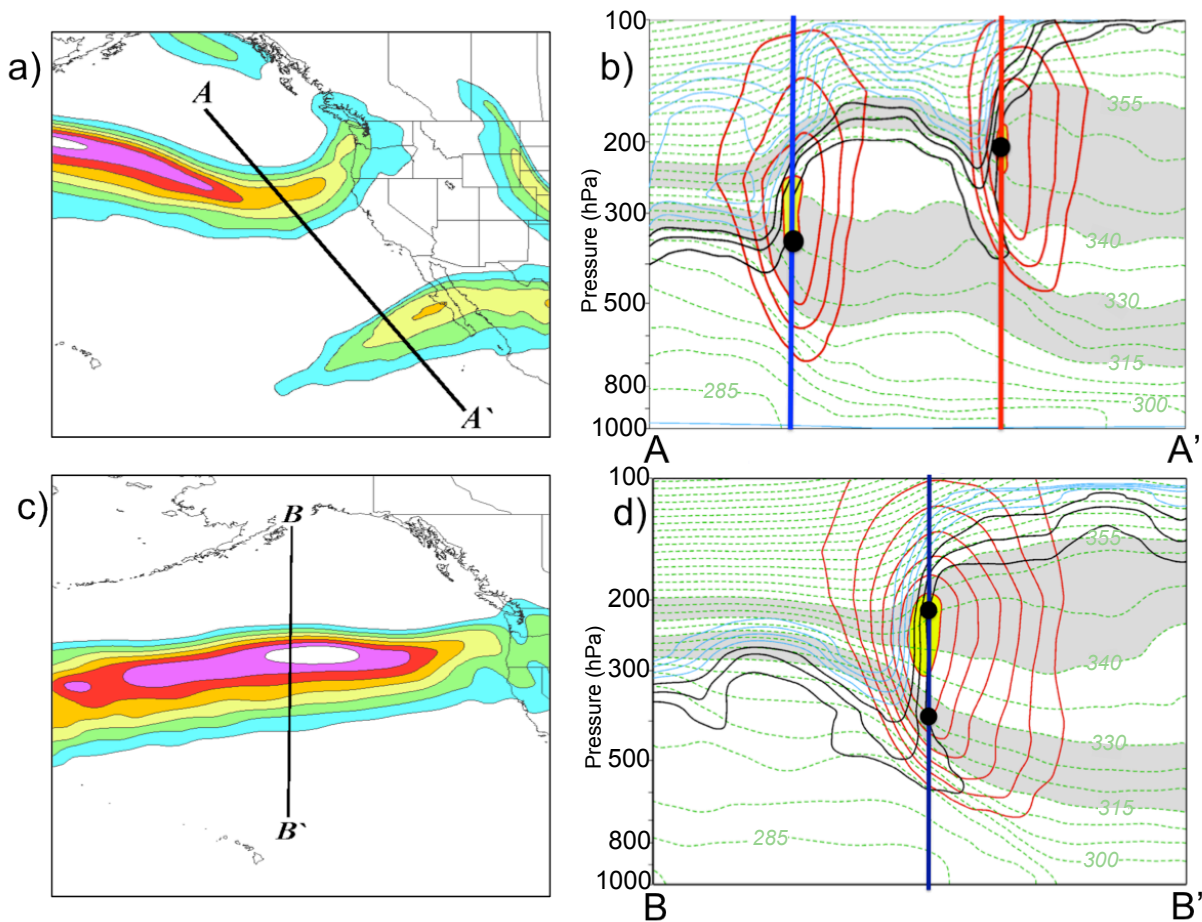


FIG. 2. From Winters and Martin (2014): a) 300-hPa isotachs shaded every 10 m s^{-1} starting at 30 m s^{-1} showing separate polar and subtropical jets near the west coast of the U.S. at 0000 UTC 27 April 2010. b) Cross section A-A' through both the polar and subtropical jet cores from panel a) with 1-, 2-, and 3-PVU surfaces contoured in black, 4-, 5-, 6-, 7-, 8-, and 9-PVU surfaces contoured in light blue, potential temperature contoured every 5 K in dashed green, and isotachs (red) every 10 m s^{-1} starting at 30 m s^{-1} . The PJ and STJ jet cores are shaded in yellow and the 315-330 and 340-355K isentropic layers (i.e., PJ and STJ isentropic layers, respectively), are shaded in grey. The blue (red) lines through a grid column with a black dot represent the identification of a polar (subtropical) jet. c) Same as panel a) but for a vertical jet superposition event at 0000 UTC 24 Oct 2010. d) Same as panel b) but for the cross section B-B' in panel c), with the PJ and STJ identifications (black dots) occurring within the same grid column indicating a jet superposition.

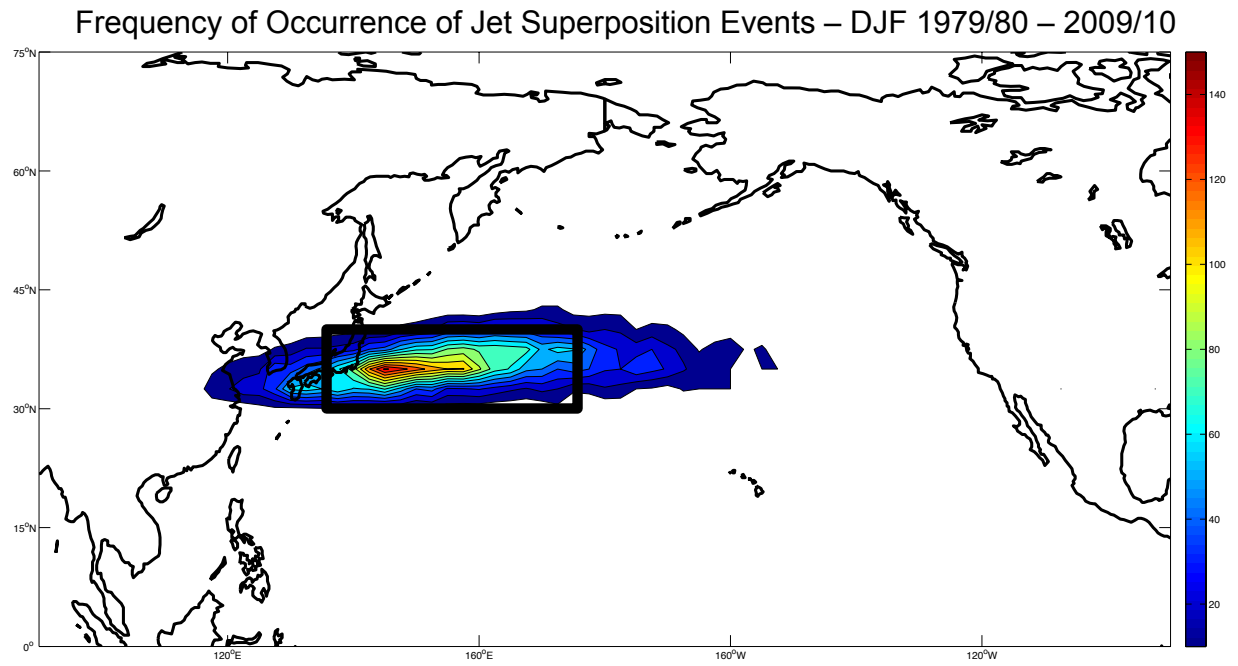


FIG. 3. Frequency of occurrence of vertical jet superposition events over the Pacific Ocean in the Northern Hemisphere during boreal winters 1979/80 - 2009/10. The black box region represents the region of interest in our study.

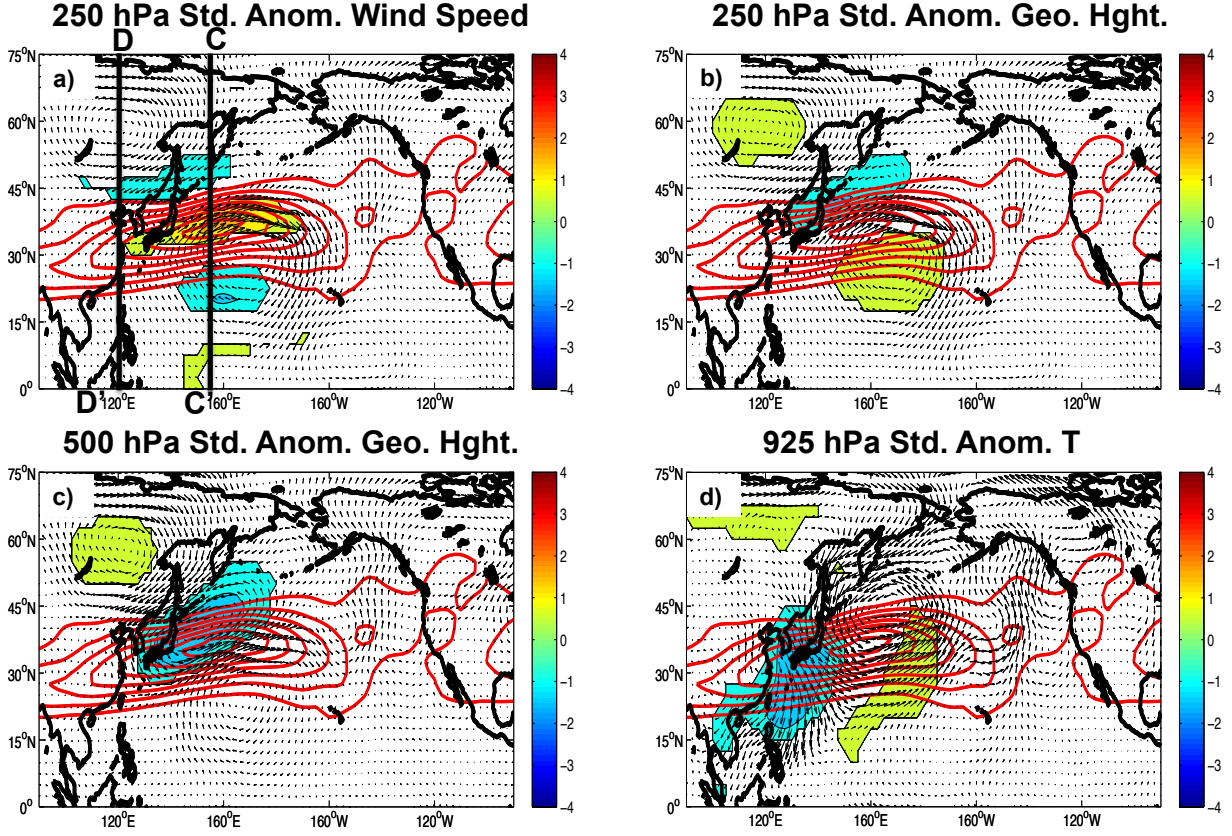


FIG. 4. Composite maps over the North Pacific ocean. a) $\vec{v}_{250, std. anom.}$ (fill; yellow (blue) colors represent values \geq (\leq) 0.5σ from climatology), b) $\phi_{250, std. anom.}$ (same fill pattern conventions as panel a), c) $\phi_{500, std. anom.}$ (same fill pattern conventions as panel a) and d) $T_{925, std. anom.}$ (same fill pattern conventions as panel a). On all maps, anomalous wind speeds at the level specified are plotted as vectors, and composite wind speed at 250 hPa is plotted as solid red contours every 10 m s^{-1} starting at 30 m s^{-1} . All maps are composite at the time of West Pacific vertical jet superposition. The cross section lines C-C' and D-D' are relevant for Figs. 7 and 8, respectively.

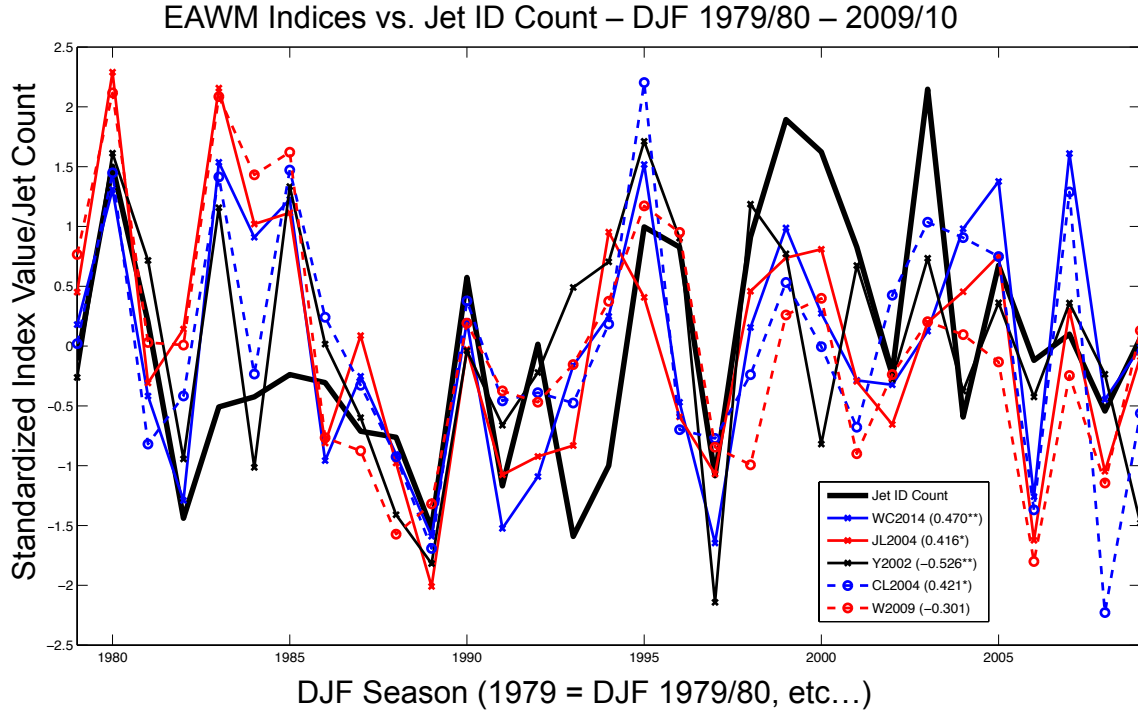


FIG. 5. Time Series of cold season standardized jet superposition ID frequency in the West Pacific box region (thick black solid line) along with 5 standardized EAWM indices for winters 1979/80 - 2009/10. Note that for the Yang et al. (2002) and Wang et al. (2009) time series plots, the time series were multiplied by -1 so that for all indices shown, positive (negative) values imply strong (weak) EAWM winters. Also included are the correlation coefficients between each EAWMI and superposition ID frequency, where values with a single (double) asterisk are significant at the 95% (99%) level (note that we assume each winter season is independent of the others such that the number of degrees of freedom = $N-2$, with $N = 31$).

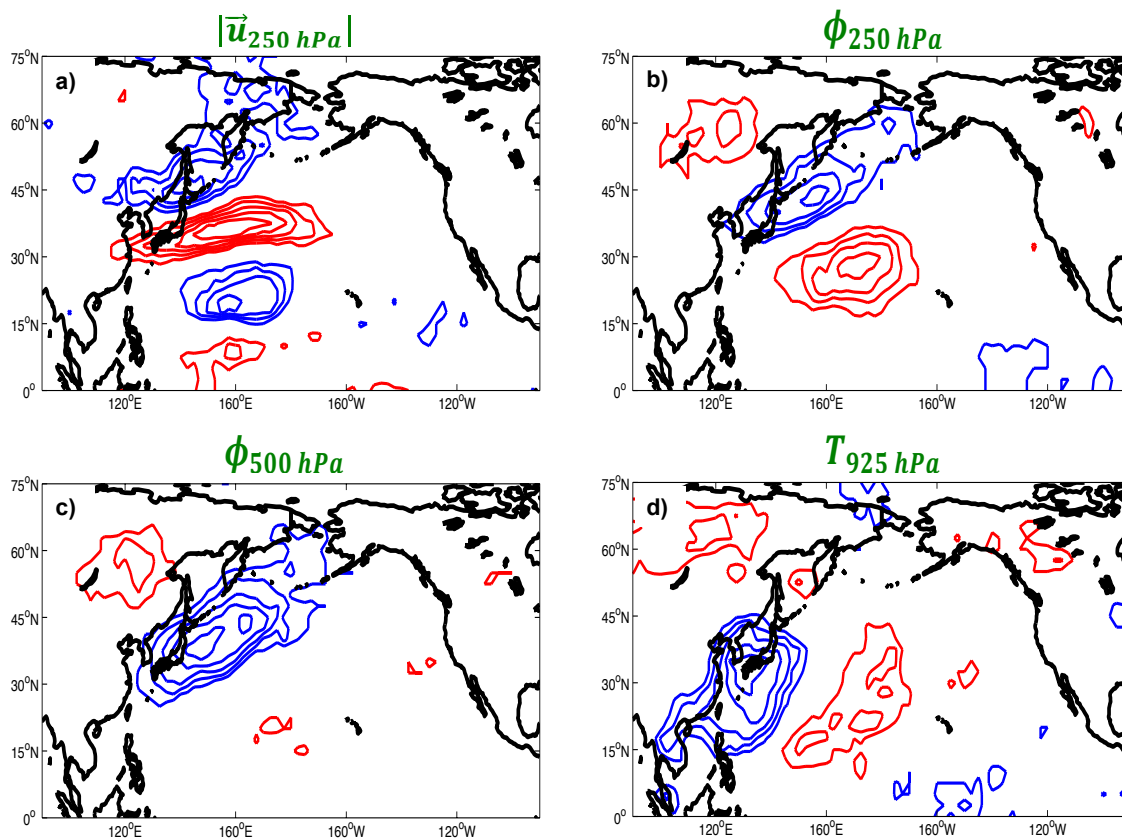


FIG. 6. Percent occurrence of each of the standardized variables in Fig. 4 for all 44 cases used in the composite. Red (blue) contours indicate regions where variable of interest with standardized value $\geq 0.5\sigma$ ($\leq -0.5\sigma$) occurs in at least 50% of cases contoured every 10%. Variables in each panel match those of Fig. 4.

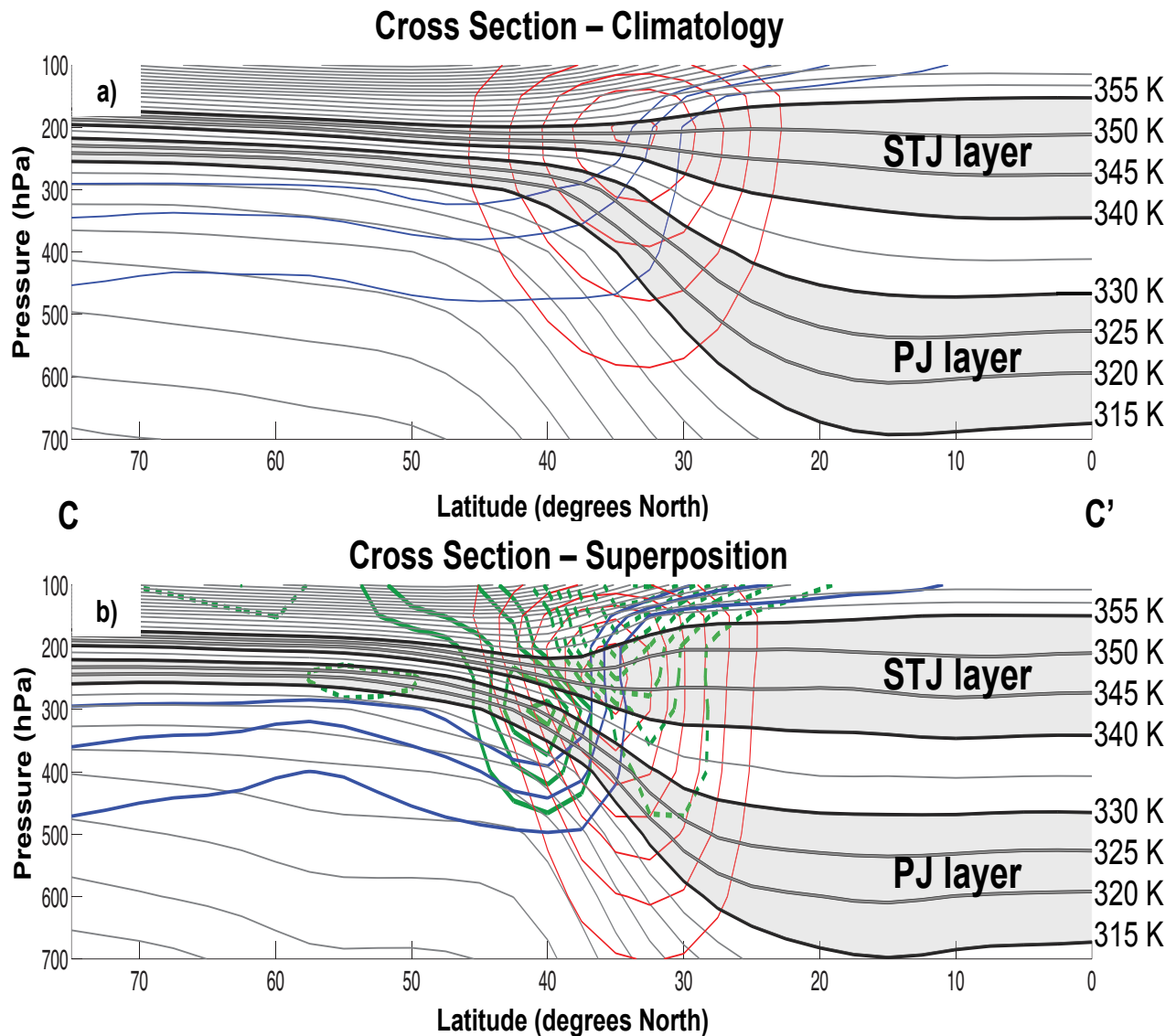


FIG. 7. a) Climatological composite cross section taken along 155°E longitude (C-C' line from Fig. 4a) of wind speed (solid red contour; 10 m s^{-1} intervals starting at 30 m s^{-1}), isentropic surfaces (solid gray contour every 5 K starting at 280 K with levels within 315-330 K and 340-355 K layers in thicker black contour, labeled and shaded in light gray) and the 1-3 PVU channel in the upper troposphere (solid blue contour; units PVU). b) Same as Fig. 7a but for the composite superposition data, including anomalous Ertel PV (solid (dashed) green contour every 0.5 PVU starting at + (-) 0.5 PVU). Note that the climatological composite cross section is computed by averaging together the climatological data for all 44 dates/times considered in this study, with the climatology for each date/time being the 31 year average at that particular time.

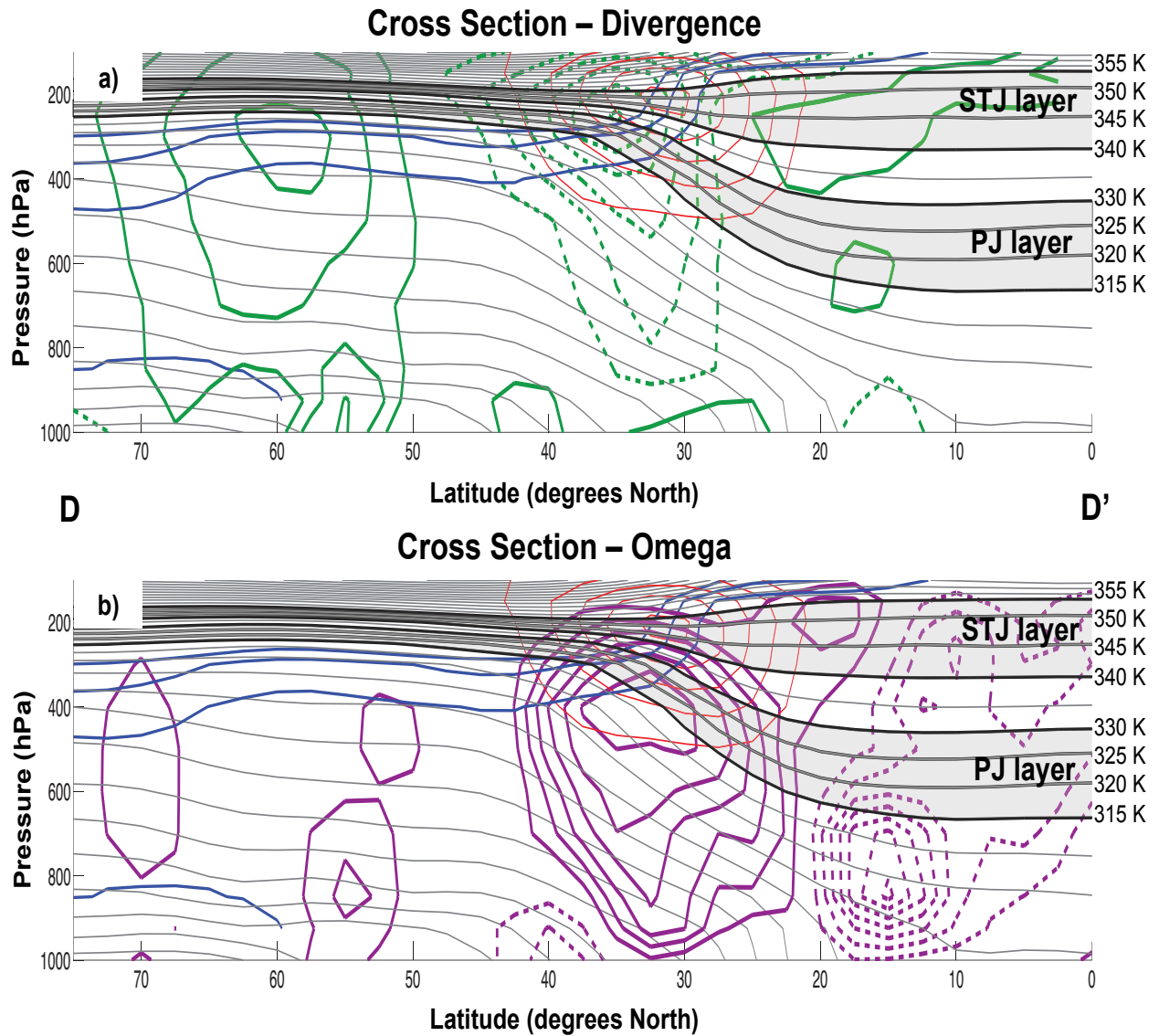


FIG. 8. Cross sections taken along 120°E longitude (D-D' line from Fig. 4a). All conventions are the same as that of Fig. 7 except that the solid (dashed) green contour represents anomalous divergence (convergence) every $0.5 \times 10^{-6} \text{ s}^{-1}$ starting at $\pm 0.5 \times 10^{-6} \text{ s}^{-1}$ in panel a and the solid (dashed) purple contour represents anomalous downward (upward) vertical motion every 0.01 Pa s^{-1} starting at $\pm 0.01^{-2} \text{ Pa s}^{-1}$ in panel b.

T-3 Days Prior to Superposition

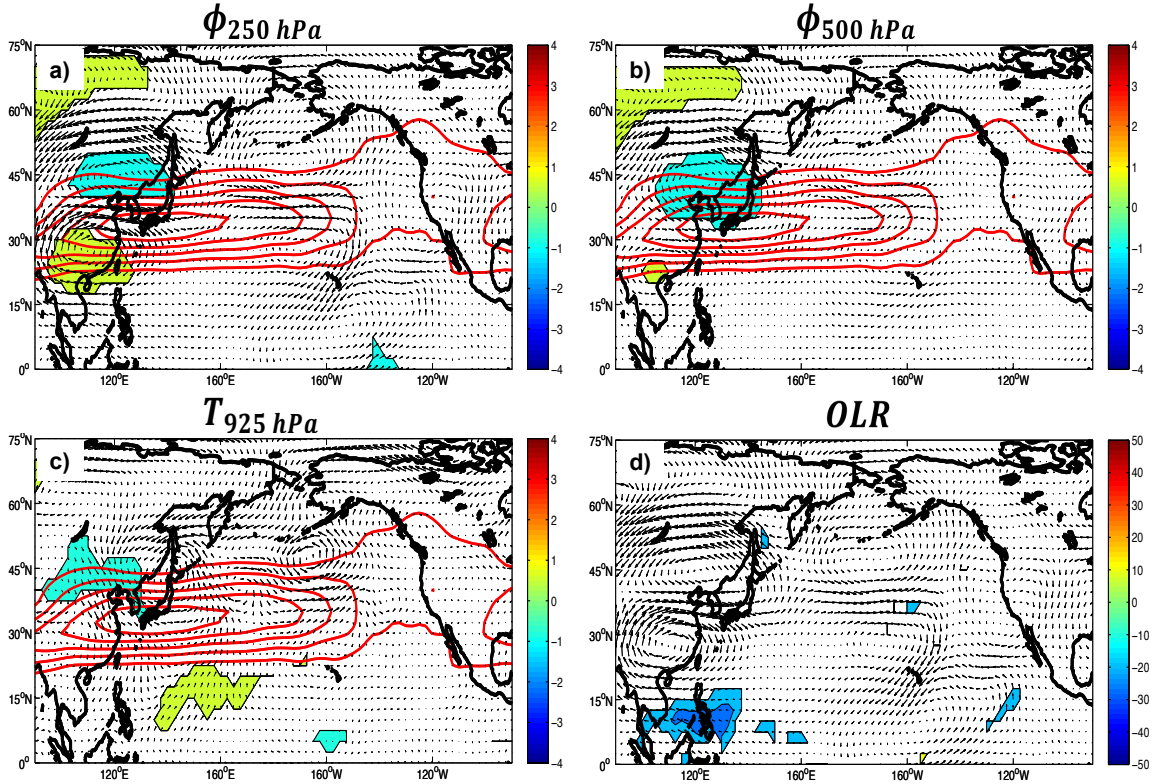


FIG. 9. Composite maps of a) $\phi_{250, std. anom.}$, b) $\phi_{500, std. anom.}$, c) $T_{925, std. anom.}$ and d) daily-averaged anomalous interpolated Outgoing Longwave Radiation (OLR) 3 days prior to composite West Pacific vertical jet superposition. Conventions are the same as Fig. 4 except for the OLR plots, where the anomalous OLR values are contoured every $10 W m^{-2}$ starting at $+ (-) 10 W m^{-2}$, and wind vectors represent 250 hPa anomalous wind ($m s^{-1}$).

T-2 Days Prior to Superposition

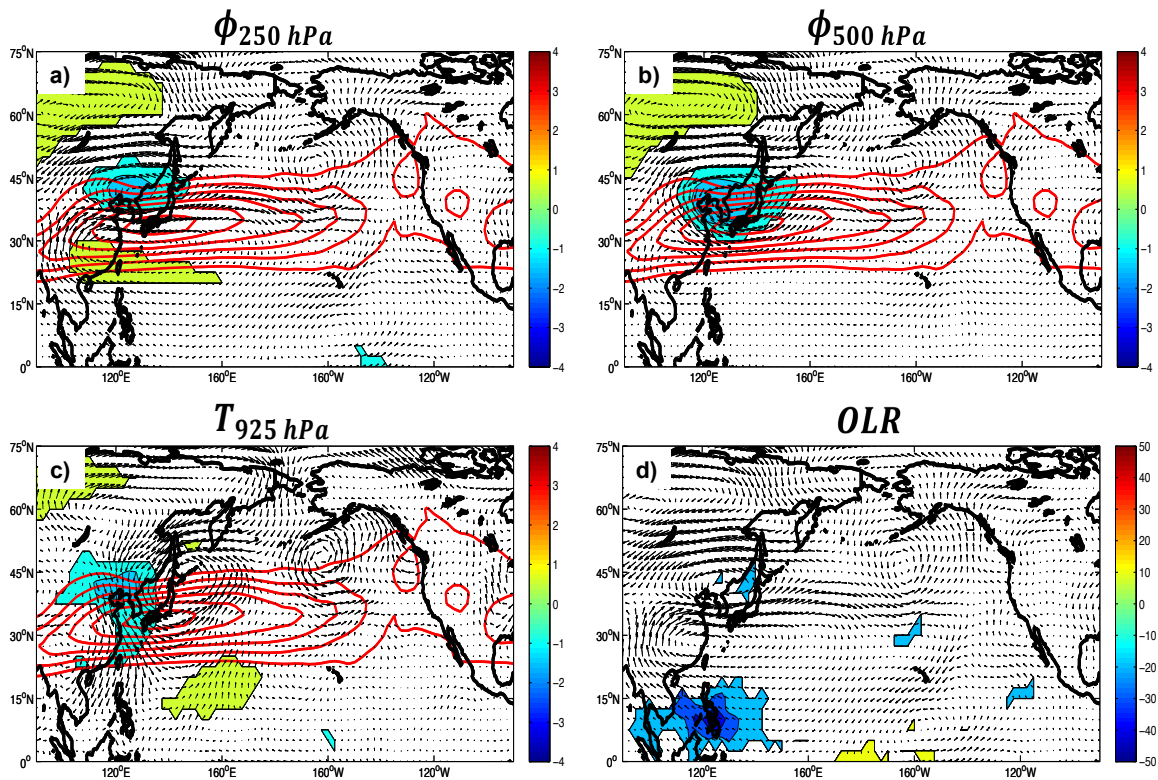


FIG. 10. Same as Fig. 9, but time prior to vertical jet superposition is 2 days rather than 3 days.

T-1 Day Prior to Superposition

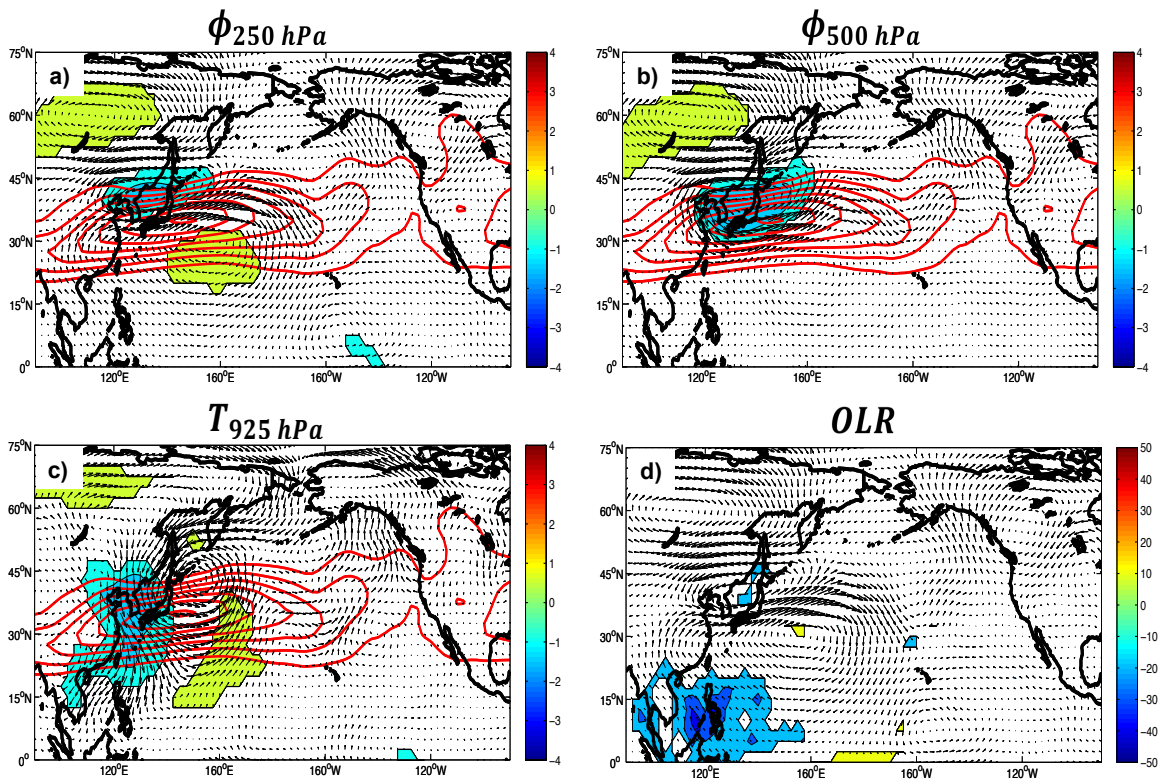


FIG. 11. Same as Fig. 9, but time prior to vertical jet superposition is 1 day rather than 3 days.

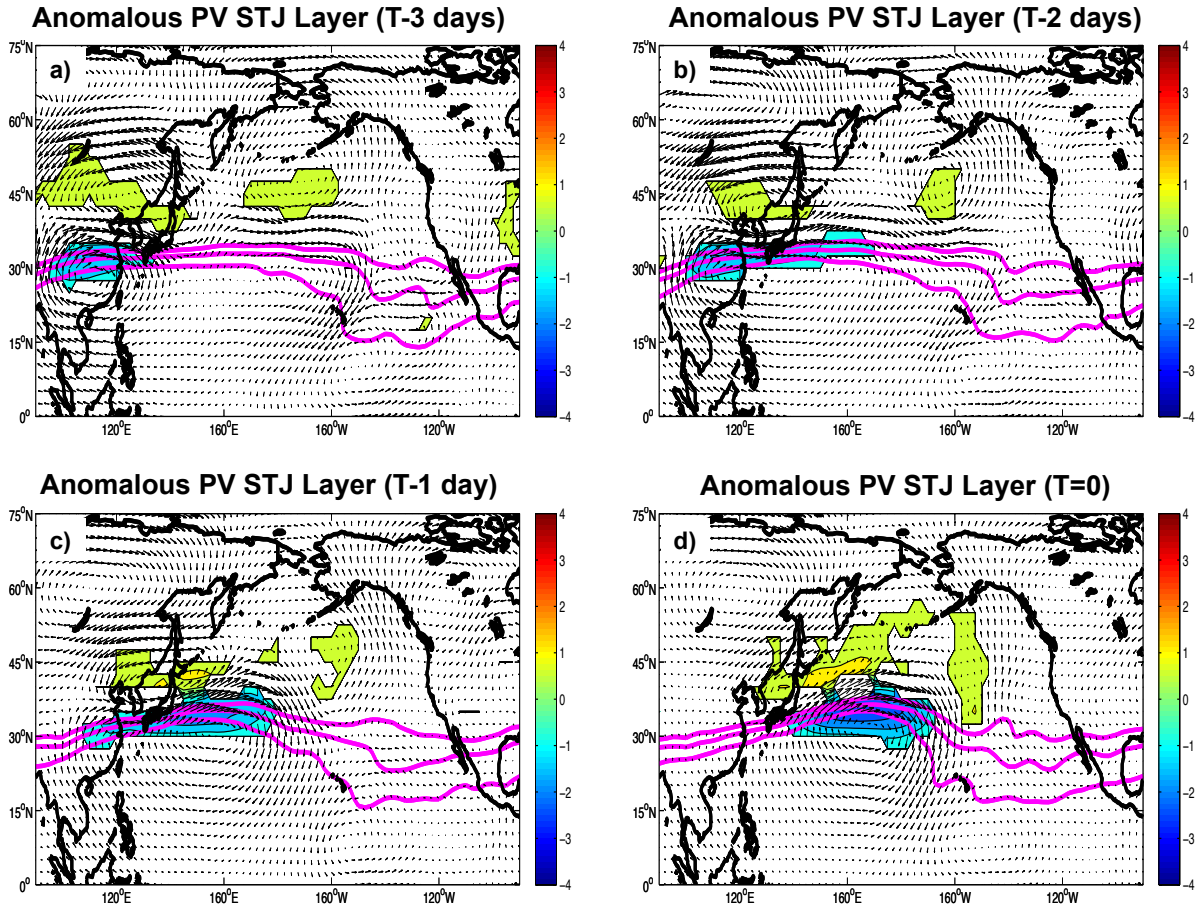


FIG. 12. Anomalous PV (PV units) within the STJ (340-355K) isentropic layer (fill pattern) at a) 3 days prior to composite superposition, b) 2 days prior to composite superposition, c) 1 day prior to composite superposition and d) at the time of composite superposition. The 1-3 PVU surfaces are contoured in solid purple. Anomalous winds within the STJ layer are shown as vectors.

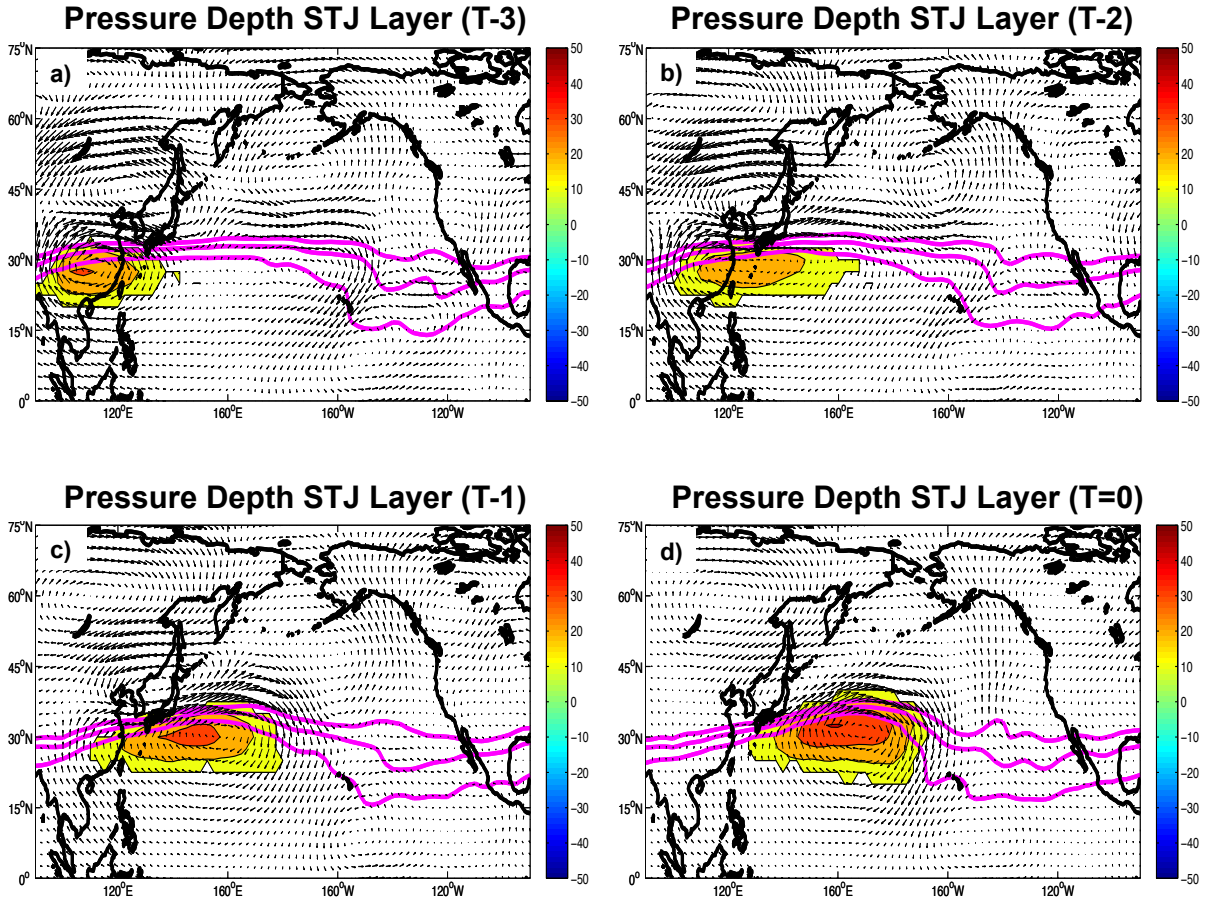


FIG. 13. Composite anomalous pressure depth within the STJ (340-355K) isentropic layer (fill pattern) at a) 3 days prior to composite superposition, b) 2 days prior to composite superposition, c) 1 day prior to composite superposition and d) at the time of composite superposition. Note that $dp = p_{340K} - p_{355K}$ for the 340-355K isentropic layer. 1-3 PVU surfaces are contoured in solid purple. Anomalous winds within the STJ layer are shown as vectors.

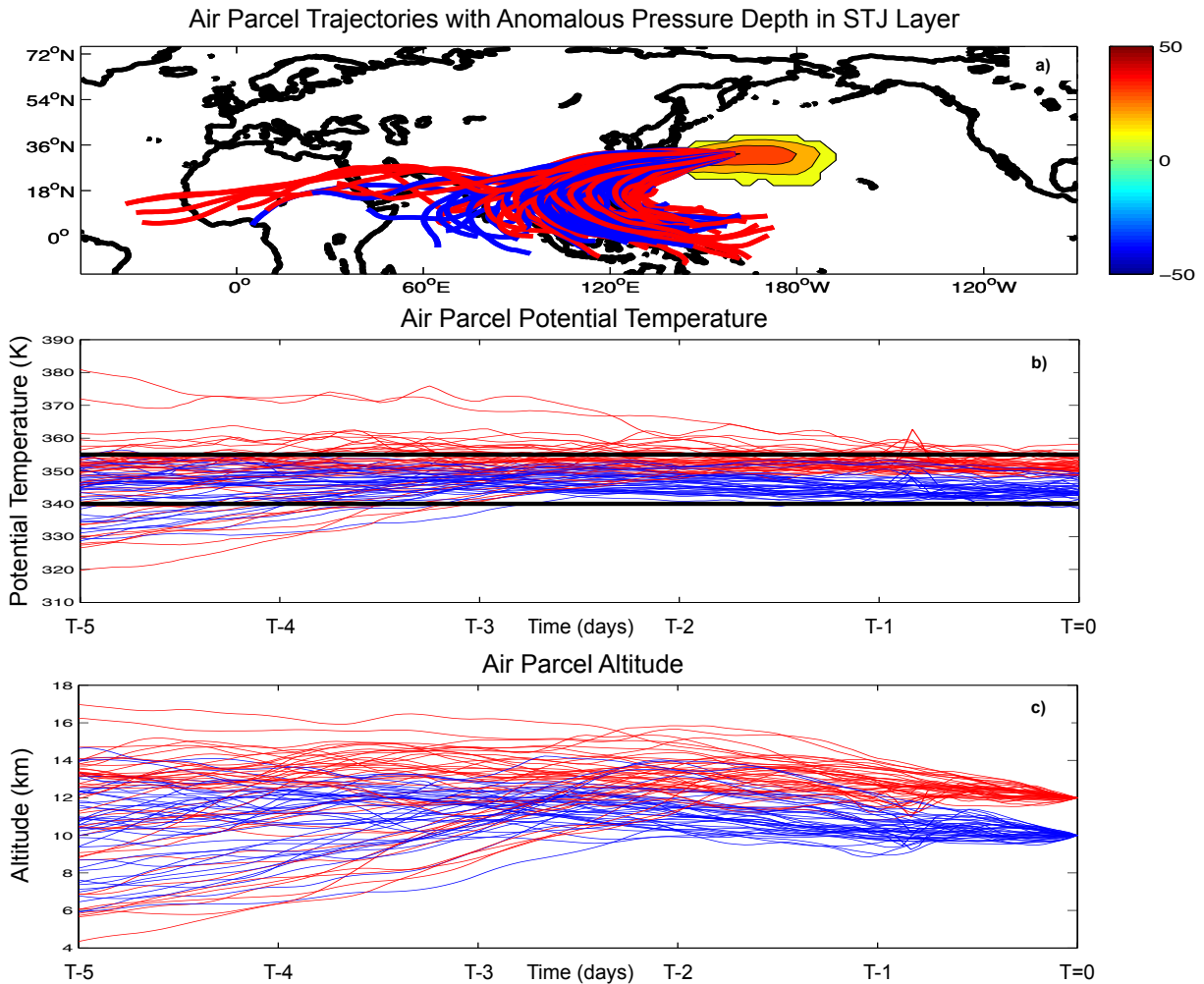


FIG. 14. a) Same as Fig. 13d, but included are ARL HYSPLIT 120 hour back-trajectories for air parcels, where the trajectories begin at the center of the anomalous pressure depth feature within the STJ isentropic layer (32.5°N , 160°E). Trajectories colored in blue (red) represent parcels with back-trajectories starting at 10 km (12 km). b) Time series of θ (K) associated with each parcel back-trajectory shown in panel a. Color conventions for the time series are same as that of the trajectories from panel a. The STJ isentropic layer lies between the solid black lines (340-355K). c) Time series of altitude (km) associated with each parcel back-trajectory shown in panel a. The color conventions are the same as panel b.

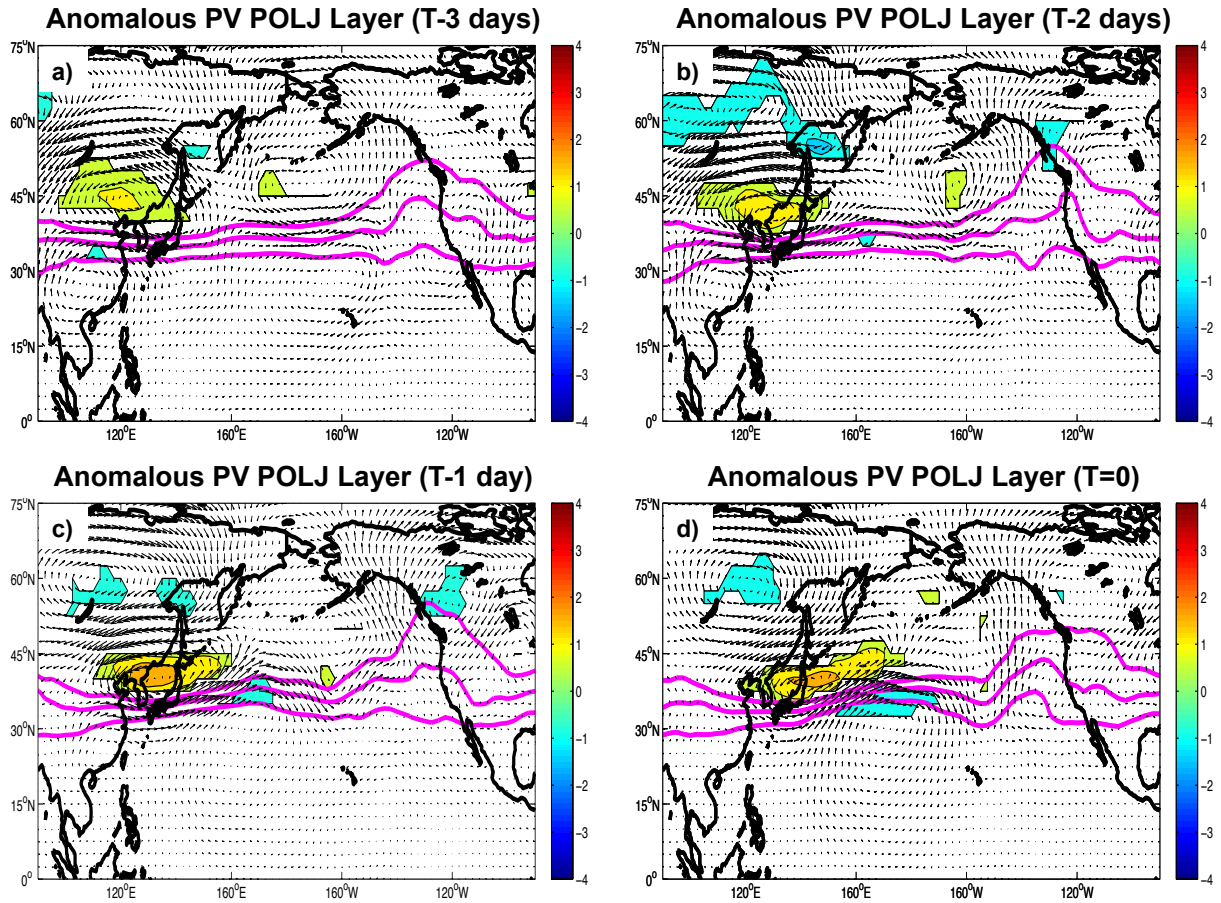


FIG. 15. Anomalous PV (PV units) within the PJ (315-330K) isentropic layer (fill pattern) at a) 3 days prior to composite superposition, b) 2 days prior to composite superposition, c) 1 day prior to composite superposition and d) at the time of composite superposition. The 1-3 PVU surfaces are contoured in solid purple. Anomalous winds within the PJ layer are shown as vectors.

Composite Geostrophic Temperature Advection and Omega – 300 hPa

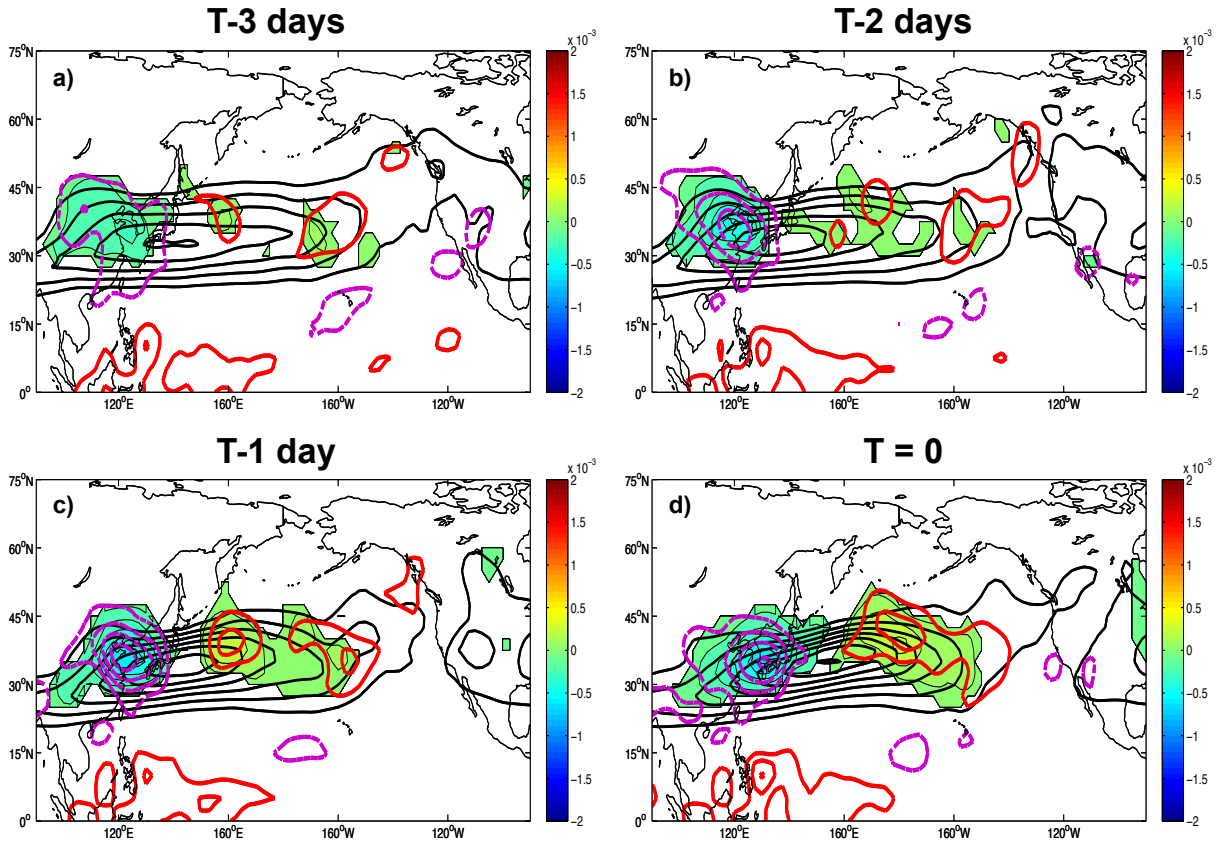


FIG. 16. 300 hPa composite geostrophic temperature advection (fill pattern; units K s^{-1}) and vertical motion (red (purple) solid (dashed) contour indicates upward (downward) vertical motion) contoured every 0.05 Pa s^{-1} starting at $+ (-) 0.05 \text{ Pa s}^{-1}$ for times a) 3 days prior to jet superposition, b) 2 days prior to jet superposition, c) 1 day prior to jet superposition, and d) at time of jet superposition. Also plotted on all panels are 300 hPa composite wind speed (black solid contour) every 10 m s^{-1} starting at 30 m s^{-1} .

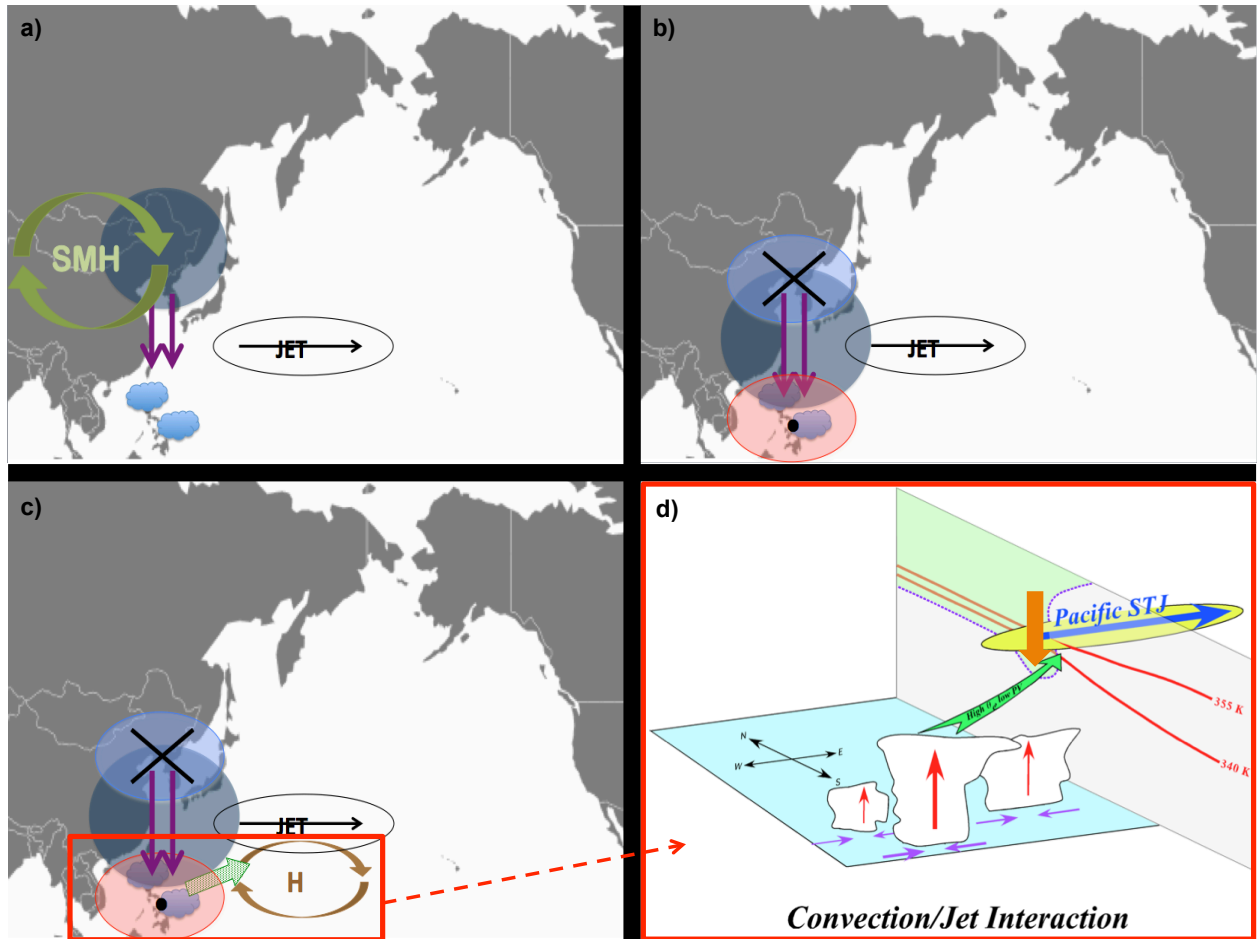


FIG. 17. Conceptual model outlining the role of tropical forcing with respect to onset of robust vertical jet superposition events in the West Pacific. In panel a), the green arrows with the abbreviation “SMH” represents the Siberian-Mongolian High, the purple arrows represent near-surface anomalous northerly winds, the blue cloud symbols represent anomalous tropical convection and the black thin circle with the westerly vector represents the approximate position of the composite jet. All features in panel a) are present 3 days prior to composite vertical jet superposition. In panel b), the blue (red) circle indicates the region of anomalous upper tropospheric convergence (divergence), with the “x” (dot) symbol representing anomalous downward (upward) vertical motion within the air column. In panel c), the brown arrows with the “H” in the center represents the anomalous geopotential height maximum feature on the anticyclonic shear side of the jet that develops 48 hours prior to composite jet superposition. The hatched green arrow represents the direction of transport of high- θ_e , low-PV air mass from the tropics towards the region where the anomalous anticyclone develops equatorward of the jet. Panel d) demonstrates the role of low-PV, high- θ_e air associated with tropical convective outflow as it is transported into the STJ isentropic layer equatorward of the superposed jet. The orange arrow represents subsidence within the jet entrance region that plays a role in the development of the deep, vertical PV wall associated with the composite superposed jet. See text for further explanation.